Available online at www.sciencedirect.com
SCIENCE DIRECT®
Deep-Sea Research I 52 (2005) 787–813
DEEP-SEA RESEARCH PART I
www.elsevier.com/locate/dsr

Time and space scales for sea surface salinity in the tropical oceans

Thierry Delcroix[a,*], Michael J. McPhaden[b], Alain Dessier[c,1], Yves Gouriou[c]

[a]IRD/LEGOS, UMR 5566, 14, Avenue Ed. Belin, 31400 Toulouse, France
[b]NOAA/PMEL, 7600 Sand Point Way NE, Seattle, WA 98115, USA
[c]IRD, US025, BP 70, 29280 Plouzané, France

Received 20 February 2004; received in revised form 15 November 2004; accepted 27 November 2004

Abstract

An unprecedented compilation of Sea Surface Salinity (SSS) data collected in the three tropical oceans (30°N–30°S) is examined for the period 1970–2003. The SSS data are derived mainly from 13 trans-oceanic Voluntary Observing Ship tracks and from 35 TAO/TRITON and 13 PIRATA mooring sites. Owing to the climatic importance of SSS, the data are used to present an overview of SSS variability, to evaluate the SSS time and space scales, and to assess the ability of the present in situ (and future satellite) observing system to adequately resolve the variability of interest. After quality control procedures, SSS is analyzed both as gridded fields (2° longitude, 1° latitude, 1 month) and as high-resolution records (0.02° latitude/longitude and one day). The gridded fields are used to describe the mean, standard deviation, and seasonal SSS cycle, as well as to estimate the characteristic scales for SSS. Results show that the monthly standard deviation of SSS mostly ranges within 0.1–0.3, except in regions with strong seasonal cycles (e.g., in the Atlantic and Pacific Inter-Tropical Convergence Zones and south of India) or prominent ENSO (El Niño Southern Oscillation) signals (e.g., in the western Pacific warm pool and in the South Pacific Convergence Zone) where standard deviations can range from 0.4 up to 1.4. The time scale for SSS is generally less than 3 months, while it reaches 4–8 months in regions where the variability is controlled mostly by ENSO. The meridional scale for SSS is generally 2–3° latitude, increasing to 4–7° latitude in the western Pacific warm pool and poleward of 10–20° latitude. The zonal scale for SSS is 15–20° longitude in the equatorial Pacific and in the South Pacific Convergence Zone (SPCZ), and 4–7° longitude along 8–10°N in the Indian Ocean. Decorrelation scales in the western Pacific warm pool tend to be smaller during La Niña time periods, with values approaching those found for the central Pacific. The signal to noise ratios are on average of the order of 1–1.5, meaning that part of the variability is not resolved from gridded fields. High-resolution records are thus used to assess the short time/space SSS variability on time and space scales shorter than the above-noted grid sizes. It is shown that the *mean* expected variability of SSS over a period of 10 days in a 1° latitude and 2° longitude box

*Corresponding author. Tel.: +33 5 61 33 30 01; fax: +33 5 61 25 32 05.
E-mail address: Thierry.Delcroix@cnes.fr (T. Delcroix).
[1]Presently retired.

0967-0637/$ - see front matter
doi:10.1016/j.dsr.2004.11.012

(i.e., the resolution requirement for the Global Ocean Data Assimilation Experiment (GODAE)) is about 0.2, with, however, notable regional differences in this value. The implications of this short time/space variability are discussed in the context of the 0.1 SSS GODAE accuracy requirement.

Keywords: Sea surface salinity; Tropical oceans; ENSO; Seasonal cycles; GODAE

1. Introduction

Sea Surface Temperature (SST) and Salinity (SSS) have been measured in the oceans for more than one hundred years. The early data were collected mainly to improve fishing capabilities. Today, SSS data are collected primarily for studying physical oceanography, the ocean's response to meteorological forcing, and climate variability.

In the tropics, most of the pre-1990 scientific studies dealing with SSS relied either on sporadic oceanographic cruises or on routine measurements obtained from Voluntary Observing Ships (VOS) (e.g., Neumann, 1969; Hires and Montgomery, 1972; Donguy and Hénin, 1976; Saur, 1980; Levitus, 1982, 1986). Thereafter, surface samples collected from VOS were progressively replaced by automatic ThermoSalinoGraph (TSG) instruments, hence improving the accuracy and the spatial resolution of the data along ship tracks (Hénin and Grelet, 1996). The location, temporal resolution, and duration of these tracks were, however, limited by commercial shipping considerations, and some climatic regions remained poorly sampled. In the 1980s, TSG were also installed at mooring sites (McPhaden et al., 1990), hence further improving the spatial extent of the measurements and most of all the temporal resolution at selected fixed points.

SSS monitoring is now part of the global ocean observing system (WCRP, 1998) and the El Niño Southern Oscillation (ENSO) observing system (McPhaden et al., 1998). At present, the bulk of the routinely obtained SSS data stems from more than a dozen regular ship tracks in the three tropical oceans (see Section 2), from TAO/TRITON (Tropical Atmosphere Ocean/Triangle Trans-Ocean Buoy Network) moorings in the Pacific (McPhaden, 1995; Kuroda and Amitani, 2001), and from PIRATA (Pilot Research Moored Array in the Tropical Atlantic) moorings in the Atlantic (Servain et al., 1998). A relatively smaller amount of SSS data further originate from infrequent research cruises, from Argo floats (Roemmich. 2000) and eXpendable Conductivity Temperature Depth (XCTD) transects (Sprintall and Roemmich, 1999).

The measurements of SSS have proven to be valuable for: (a) describing and understanding climate variability in the Pacific (Delcroix and Hénin, 1991), Atlantic (Dessier and Donguy, 1994), and Indian (Donguy and Meyers, 1996) oceans, (b) hypothesis testing of physical processes (Delcroix and Picaut, 1998; Delcroix and McPhaden, 2002), (c) assessing numerical model performance (Vialard et al., 2002), (d) improving the estimation of vertical salinity profiles and so quantifying the role of salinity on sea level and geostrophic currents (Kessler and Taft, 1987; Maes, 1998; Ueki et al., 2002), (e) improving ENSO prediction lead time in statistical models (Ballabrera-Poy et al., 2002), (f) improving modeled mixed-layer representation via data assimilation (Durand et al., 2002), (g) assessing the relevance of paleo-salinity data (Le Bec et al., 2000), and (h) reconstructing CO_2 flux at the ocean–atmosphere interface (Loukos et al., 2000). Futhermore, we can anticipate that the routinely collected and real-time transmitted in situ SSS data will be crucial for validating future European (Kerr et al., 2001) and USA/Argentina (Koblinski et al., 2003) satellite missions which will provide global SSS coverage.

Given the large number of in situ SSS observations presently available from complementary sources, as well as the future availability of remote observations, the time is right to: (1) provide an overview of SSS variability for the global tropics, (2) systematically evaluate the time and space

scales of SSS variability, and (3) assess the ability of the present in situ (and future remote) measurements to adequately resolve the variability of interest. Aside from expanding our knowledge about SSS, this effort will provide further guidance for mapping irregularly sampled observations via objective analysis, and it will also help us in assessing how sparse sampling and averaging techniques could affect interpretation of the observations. Similar studies were done in the past for variables other than SSS: for eXpendable Bathy Thermograph (XBT)-derived temperature in the Pacific (White and Berstein, 1979; White et al., 1982; Kessler and Taft, 1985; Meyers et al., 1991), for TAO-derived temperatures (Kessler et al., 1996) and winds (Mangum et al., 1992), and for the in situ and altimeter-derived sea level (Kuragano and Kamachi, 2000). A preliminary study was done for SSS (Lagerloef and Delcroix, 2001) but the analysis was limited to the western Pacific Warm Pool only.

The remaining of the paper is organized as follows. Section 2 describes the data, their validation and processing. Section 3 presents an overview of mean, standard deviation and seasonal SSS changes, section 4 discusses the time and space scales and the signal to noise ratio for SSS, and section 5 presents small-scale SSS changes and related sampling and averaging issues. The last section discusses conclusions.

2. Data collection and processing

2.1. Data collection

The original SSS data, about 4.3 million records, originate from a combination of (1) surface samples collected via VOS programs, (2) measurements taken by TSG installed onboard VOS and research vessels, (3) TSG measurements from TAO/TRITON and PIRATA moorings, and (4) near-surface hydrocasts, salinity temperature depth (STD) and conductivity temperature depth (CTD) measurements collected during research cruises. These have been described in detail in previous publications, and only a short summary is given below. (Note that we did not use XCTD and Argo data because they are relatively few in number. The Argo data are, moreover, widely scattered in space and time, which adds complication to the analysis procedures used in this study.)

The surface samples come chiefly from IRD (*Institut de Recherche pour le Développement,* formerly ORSTOM, *Office de la Recherche Scientifique et Technique Outre Mer*) VOS programs operated from Nouméa, New Caledonia, for the Pacific and Indian oceans data (Donguy and Hénin, 1976; Donguy and Meyers, 1996) and from Brest, France, for the Atlantic ocean data (Dessier and Donguy, 1994). They started to be routinely collected in 1969 for the Pacific and in 1977 for the Indian and Atlantic Oceans, then were greatly reduced in number or phased out completely in the first half of the 1990s. The samples were collected every 3–6 h, yielding a 0.5–2° resolution along the tracks depending on the ship speed. All measurements were qualitatively checked by scientists through procedures which, for each voyage, verified climatic limits and internal consistency of positions and SSS values. The accuracy of these data are limited, however, by improper sealing of water samples in buckets, by possible contamination from rain or evaporation during sampling (often carried out from 20 to 30 m high bridges), and by possible salt deposit in buckets. These effects have been discussed in many publications (see, for example, Reverdin et al., 1994a), and the accuracy of surface samples is believed to be of the order of 0.1.

The TSG underway measurements originate for the most part from VOS programs which have been operated by IRD since 1991 in the Pacific and 1995 in the Atlantic oceans to replace bucket sampling. Some of the ships providing data in the tropical Pacific steam around the world and so provide additional data in the tropical Indian and Atlantic Oceans. On average, each selected ship provides one to three sections per season along a regular track. The SSS measurements are based on Seabird SBE-21 instruments installed in the engine room; they are obtained every 15 s and median values over 5 min are stored yielding an along track resolution of about 0.02°. After quality control procedures, the SSS accuracy is believed to be of the order of 0.02 (Hénin and Grelet, 1996;

Prunier-Mignot et al., 1999). However, when 5-min apart measurements performed before and after cleaning of the sensors during ship calls were compared, differences in excess of 0.1 were sometimes observed for long voyages (>1 month). These differences, reflecting scouring or fouling effects on salinity sensors, were not quantified before year 2000 and not reported systematically after this date in TSG date bases; they thus constitute an additional source of error that cannot be rigorously quantified. Some TSG data are also collected from vessels servicing the TAO/TRITON and PIRATA moorings, with one to two cruises per year since the mid-1990s along several track lines (Johnson et al., 2002a; Kashino et al., 2001; Grelet et al., 2003). Most of these cruise-derived SSS data were further calibrated with concurrent CTD measurements so that their accuracy is probably better than 0.02.

Moored TAO/TRITON and PIRATA salinity measurements were made with three related instruments: the Seabird SBE-16 Seacat, the Seabird SBE-37 Microcat, and the Pacific Marine Environmental Laboratory (PMEL)-built temperature-conductivity (TC) module. All three instruments use the same Seabird conductivity cell. Temperature and conductivity were sampled at intervals that varied from 5 to 60 min, depending on period and location. Deployments typically were 6–12 months in length, and in most cases sensors were calibrated before and after deployment. CTD casts near the moorings were also made for calibration purposes. Moorings deployed with multiple instruments in the mixed layer allowed for detection and possible correction of sensor drift via comparison of instruments at neighboring depths. Moorings deployed with only a surface sensor relied primarily on pre- and post-calibration information and CTD data for quality evaluation.

The most comprehensive analysis of moored salinity data quality is that of Freitag et al. (1999) for Seacat data collected during Tropical Ocean Global Atmosphere, Coupled Ocean Atmosphere Response Experiment (TOGA-COARE); see WCRP, 1990). This analysis documented possible biases due to electronic drift, conductivity cell scouring, and biological fouling of the sensors. However, with post-processing for quality control purposes, errors in the moored salinity time series were generally reduced to about 0.02. Microcat and TC data are expected to have similar error characteristics because they derive from the same conductivity cells as used in Seacats deployed during COARE. Recent Seacat, Microcat, and TC intercomparisons in the western Pacific warm pool and preliminary analyses of salinity data from throughout the tropical Pacific and Atlantic generally support this conclusion. However, in biologically productive regions such as in the equatorial cold tongue of the eastern Pacific and Atlantic, measurement uncertainties may be higher. A comprehensive update of Freitag et al. (1999) is underway to quantify the error characteristics of all the sensors used in all areas sampled by the TAO/TRITON and PIRATA arrays.

Finally, 0–10 m salinity data originating from hydrocasts, STD and CTD were also considered. Most of these were obtained from the 2001 version of the World Ocean Atlas (WOA) data base (see Stephens et al., 2002), with data dating back to the early 20th century. To ensure the maximum data available and include recently collected measurements, IRD and NOAA/PMEL CTD archives were added to the SSS database. The research cruise STD and CTD SSS measurements are believed to be of higher accuracy than other SSS data since they were obtained by research scientists with highly accurate instruments.

2.2. Data processing

Aside from the mooring-derived data, the three types of SSS data (bucket samples, VOS-derived, and cruise-derived measurements) originate from 13 different databases. We therefore looked for possible duplicates whose detection was based on identical SSS values and space–time locations: about 0.02% of the data were so removed. In addition to the quality control performed by the data originators, we eliminated about 0.02% of data through standard statistical tests rejecting values based on 5, 4, and 3.5 standard deviations computed in 5° longitude and 1° latitude boxes. The spatial and temporal distributions of the remaining SSS data are shown in Fig. 1.

In view of the space–time distribution of the VOS data, we restrict our investigation to the 1970–2001 period, and select 11 quasi-north–south (NS)-oriented and 2 quasi-east–west (EW)-oriented well-sampled tracks (see Fig. 2). These were chosen to enable analysis of SSS time series over long time periods, with 10 out of 13 tracks having SSS time series in excess of 20 years. In the following, each track will be named according to the nomenclature of the international Ship Of Opportunity Program Implementation Panel (SOOPIP). One exception will be for the so-called AX20 shipping track running from Europe to French Guyana which actually includes two tracks separated by about 10° longitude representing the southward or northward voyages: only the best-sampled westernmost track will be considered here and named AX20-W. Additional information about the selected tracks and time periods is given in Table 1. In addition, we have selected for analysis 35 mooring sites in the Pacific covering the 1988–2003 period, and 13 sites in the Atlantic covering the 1998–2003 period. At these mooring sites (Fig. 2 and Table 2), SSS record lengths generally exceed 2 years.

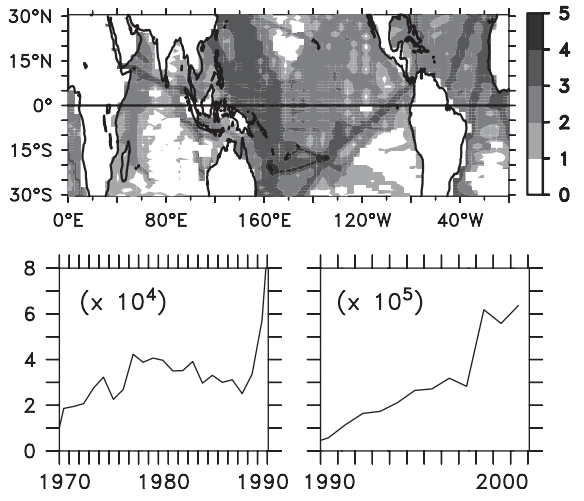

Fig. 1. (top) Number of SSS observations per 5° longitude and 1° latitude rectangle, expressed in decimal logarithm scale, as obtained from surface samples, TSG and cruise-derived measurements during 1970–2001. Note that the darkest lines denote shipping line equipped with TSG instruments. (bottom) Number of SSS observations per year. Note the different horizontal and vertical scales on the two bottom panels.

As noted above, the VOS-derived SSS data originate from different instruments and measurement methods so that the question arises as to how to mix these different data sets. Taking CTD measurements as a reference, past studies have shown that bucket samples are biased high by 0.1 on average, whereas TSG measurements are biased low by 0.02 (see, for example, Delcroix

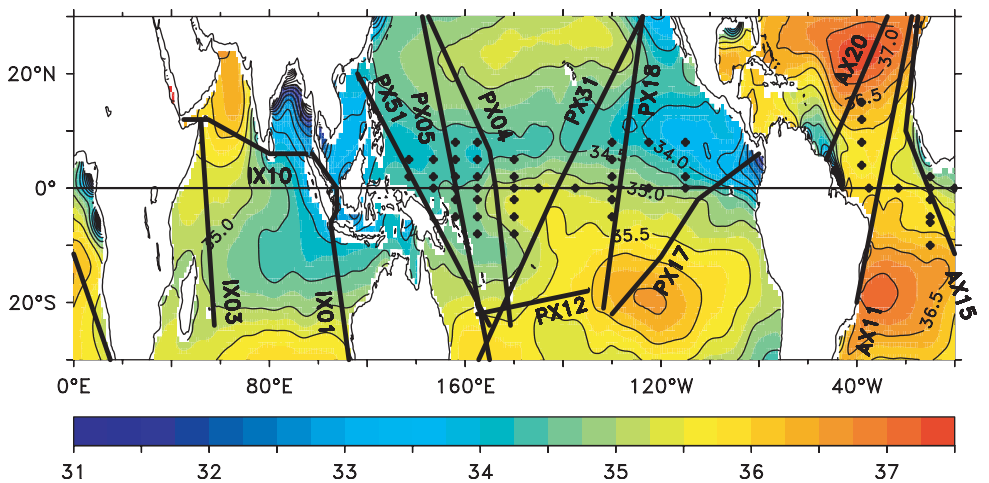

Fig. 2. Long-term mean SSS in the tropical oceans (data from Stephens et al., 2002). Over plotted as heavy lines are the 11 quasi-NS-oriented and 2 quasi-EW-oriented well-sampled shipping lines (named IX03, IX10, etc., see Table 1). The stars denotes the TAO/TRITON and PIRATA mooring where most SSS record lengths exceed 2 years.

Table 1
Main features of the 13 trans-oceanic ship tracks drawn schematically in Fig. 2

Track name	From–to Equatorial crossing (if any)	Selected observations	Number of obs. (K)
IX03	La Reunion–Gulf of Aden Equatorial crossing at 53°E	1978–1996: 20°S–13°N	15.3
IX10	Malacca Strait–Gulf of Aden No equatorial crossing	1977–1985: 45°E–53°E	0.9
		1986–1991: 45°E–95°E	3.5
		1992–1997: 51°E–95°E	27.0
		2000–2001: 45°E–95°E	59.3
IX01	SW Australia–Malacca Strait Equatorial crossing at 107°E	2000–2001: 30°S–7°N	30.2
PX51	New Caledonia–Taiwan Equatorial crossing at 142°E	1970–1978: 23°S–03°S	30.3
		1979–1982: 23°S–10°S	7.9
		1983–1984: 23°S–10°N	5.4
		1985–1989: 23°S–10°S	7.6
		1990–1991: 23°S–22°N	25.9
		1992–1993: 23°S–13°N	53.7
		1994–2001: 22°S–22°N	672.7
PX05	New Caledonia–Japan Equatorial crossing at 155°E	1970–1972: 22°S–10°N	15.1
		1973–1984: 30°S–30°N	73.2
		1985–1991: 30°S–20°N	48.3
		1992–2001: 22°S–30°N	708.0
PX04	Fiji–Tarawa–Japan Equatorial crossing at 172°E	1973–1981: 22°N–30°N	3.4
		and 23°S–15°S	3.9
		1982–1983: 23°S–30°N	2.5
		1984–1991: 23°S–20°N	10.6
		1992–2001: 23°S–30°N	26.5
PX12	New Caledonia–French Polynesia No equatorial crossing	1975–2001: 165°E–150°W	514.8
PX31	New Caledonia–California Equatorial crossing at 162°W	1973–1975: 30°S–15°S	3.1
		1976–1991: 30°S–30°N	80.5
		1992–2001: 30°S–15°S	192.3
PX18	French Polynesia–California Equatorial crossing at 140°W	1980–1991: 21°S–30°N	184.6
PX17	French Polynesia–Panama Equatorial crossing at 97°W	1975–1978: 3°S–7°N	2.7
		1979–1997: 22°S–7°N	46.3
		1999–2001: 5°S–7°N	35.9
AX20-W	Europe–French Guyana No equatorial crossing	1977–1983: 5°N–30°N	2.2
		1985–1986: 5°N–30°N	0.5
		1992–1994: 5°N–30°N	2.2
		1995–1999: 5°N–30°N	48.7
AX11	Europe–SE Brazil Equatorial crossing at 32°W	1977–1986: 20°S–30°N	6.9
		1986–1992: 20°S–20°N	9.2
		1995–2001: 20°S–30°N	125.3
AX15	Europe–South Africa Equatorial crossing at 8°W	1977–1987: 30°S–30°N	6.3
		1988–1996: 20°S–20°N	15.5
		1997–1998: 30°S–20°N	15.5
		1999–2001: 30°S–30°N	55.6

and Hénin, 1991; Hénin and Grelet, 1996; Bingham et al., 2002). An analysis of about 1100 TSG-derived and bucket sample-derived SSS measurements collected simultaneously on VOS during 2000–2002 confirmed the −0.12 mean difference between the two techniques, provided that we discard obvious erroneous measurements with differences in excess of ±0.5 (10% of the data

Table 2
Means values of SSS standard deviations computed over 10- and 30-day (in parentheses) periods at TAO/TRITON and PIRATA mooring sites

	137°E	147°E	156°E	165°E	180°	170°W	155°W	140°W	125°W	110°W
8°N			0.07 (0.10)	0.08 (0.13)					0.12 (0.14)	0.09 (0.21)
5°N		0.09 (0.13)	0.09 (0.12)	0.11 (0.15)	0.11 (0.16)			0.10 (0.14)		
2°N	0.08 (0.11)	0.10 (0.15)	0.10 (0.15)	0.11 (0.15)	0.07 (0.11)			0.06 (0.10)		0.12 (0.18)
EQ.		0.12 (0.19)	0.09 (0.13)	0.08 (0.11)	0.08 (0.11)	0.07 (0.12)	0.06 (0.09)	0.07 (0.10)	0.12 (0.15)	0.13 (0.19)
2°S			0.10 (0.15)	0.10 (0.14)	0.09 (0.12)			0.07 (0.09)		
5°S			0.10 (0.14)	0.12 (0.17)	0.11 (0.17)			0.04 (0.07)		
8°S				0.10 (0.14)	0.11 (0.16)					
	10°S	6°S	5°S	2°S	EQ	2°N	4°N	8°N	12°N	15°N
38°W							0.10 (0.14)	0.12 (0.21)	0.08 (0.15)	0.05 (0.08)
35°W					0.10 (0.14)					
23°W					0.13 (0.20)					
10°W	0.04 (0.07)	0.06 (0.11)	0.07 (0.11)	*0.08 (0.16)*	0.15 (0.20)	*0.16 (0.20)*				
0°W					0.16 (0.23)					

Values in *italics* at 10°W, 2°S and 2°N, were obtained from record lengths less than one year.

with 5% originating from the same ship). Hence, we subtracted 0.1 from all bucket measurements, and added 0.02 to all VOS-derived TSG measurements. In doing so, we understand that some bias errors may still remain. In fact, as a makeshift solution, the prescribed corrections were considered as constant, whereas concurrent CTD, bucket and TSG measurements performed during oceanographic cruises have shown that such corrections could vary with time. Also, the technique used to obtain the data was sometimes not documented, and no correction was applied in this latter case. Nevertheless, the lack of an obvious 1992 shift in SSS time series from well sampled regions when bucket samples were systematically replaced by TSG measurements, gives us some confidence in using these constant corrections.

Another possible source of error arises from the grouping of scattered SSS data into mean tracks of 2–10° width. Given the present rather-poor capability of forced models in realistically simulating SSS changes, it is unlikely that they can help to estimate such error, as was done for XBT temperature data (McPhaden et al., 1988). Zonal and meridional decorrelation scales computed below from VOS and mooring data suggest, however, that grouping data over our mean tracks should not bias our conclusions too much.

To reach our first objective, which is to provide an overview of SSS variability in the tropics, we gridded the data in time and space in the following way. For the quasi-NS- (EW-) oriented ship tracks, the grid element sizes were chosen as $dy = 1°$ latitude ($dx = 2°$ longitude) and $dt = 1$ month. These were adopted to include a sufficient number of SSS measurements within a grid element (>5, on average), the limiting factor being the relatively poor time/space resolution of the bucket measurements. The median of all SSS values within a grid element was first computed. We chose to work with median values instead of mean values to reduce the potential effects of outliers in the data. A Laplacian interpolation scheme was then used to fill the grid in using neighbor points (see, Delcroix and Hénin, 1991). Data gaps exceeding three times the grid element sizes, i.e., 3 months, 3° latitude or 6° longitude, were not filled in. For consistency, the median values over 1 month were computed as well from all mooring-derived daily SSS data. Sensitivity tests showed that using monthly means or monthly medians does not change our conclusions significantly.

3. Overview of mean and seasonal variability

In this section, we present an overview of the mean, standard deviation and seasonal SSS cycle. To compare these quantities for different regions,

it would have been preferable to analyze time series covering a common long period. As shown in Table 1, there is actually no time period common to all the data, so we chose to compute all quantities in using the selected observations as displayed in Table 1 for the ship tracks, and the longest available periods for the mooring sites. As all but one ship track include 12–32 years of data, we believe that the derived climatologies will be robust, except possibly for the eastern Indian ocean (IX01), where only 2 years of data (2000–2001) are analyzed.

The mean SSS (Figs. 3–6) exhibits the well-known large scale features described in previous articles for the global (Levitus, 1986; Boyer and Levitus, 2002), tropical Indian (Donguy and Meyers, 1996), tropical Pacific (Delcroix et al., 1996) and tropical Atlantic (Dessier and Donguy, 1994) Oceans. It is to the first-order reminiscent of the mean distribution of the Evaporation minus Precipitation (E−P) budget (Oberhuber, 1988; Boyer and Levitus, 2002); note, however, that additional influences must be considered. For example, as discussed by Delcroix and Hénin (1991) for the tropical Pacific ship tracks, horizontal salt advection can account for the small latitudinal shift between the observed SSS minima (Figs. 4 and 5) and the maximum P−E associated with the Intertropical Convergence Zone (ITCZ) and South Pacific Convergence Zones (SPCZ). Likewise, horizontal salt advection by the mean ocean circulation plays a significant role in affecting the mean SSS distribution in the three tropical oceans (Johnson et al., 2002b; Mignot and Frankignoul, 2003; Han and McCreary, 2001). In addition, river runoff further affects the mean SSS distribution at regional scales, as is clearly visible in Fig. 2 off the Amazon and Congo rivers and in the northern Bay of Bengal (Dessier and Donguy, 1994; Masson and Delecluse, 2001; Boyer and Levitus, 2002; Rao and Sivakumar, 2003).

Basin-scale maps of SSS standard deviations based on a subset of our observations in the tropical Pacific and Indian oceans can be found in Delcroix et al. (1996) and Rao and Sivakumar (2003), respectively. For the tropical Atlantic, a global map showing the standard deviation of monthly mean SSS fields about the annual mean (ignoring lower frequency variations) is given by Boyer and Levitus (2002). In general agreement with these references, Figs. 3–6 indicate that the SSS standard deviation ranges from 0.2 to 1.4. The largest values are found in the Indonesian Archipelago (track IX01), to the southeast of India (track IX10), east of Panama (track PX17), in between the Amazon and Orinoco river mouths (track AX20-W), and under the Atlantic ITCZ (tracks AX11, AX15). Relative maxima of SSS standard deviations also show up for the tracks located in the central Pacific (track PX31, PX18) at the position of the mean ITCZ and SPCZ.

The right-hand panels in Figs. 3–6 show the percent of variance in monthly time series explained by the seasonal SSS cycle, so as to assess how representative this cycle is of the total signal. Results indicate that there are regions in the western half of the tropical Pacific (tracks PX51, PX05, PX04, PX12) where the seasonal SSS cycle accounts for less than 25% of the total SSS variance, reflecting the strong regional influence of ENSO (see Delcroix, 1998; Gouriou and Delcroix, 2002). In contrast, the seasonal cycle is a major signal in most of the Indian Ocean and in the Pacific and Atlantic convergence zones, accounting for at least 50% of the total variance.

The middle panels in Figs. 3–6 show the monthly mean seasonal cycle for each track. They indicate that the SSS is saltier during boreal fall north of Madagascar (track IX03) at times of positive E−P, and in the southeastern Arabian Sea (track IX10) when the clockwise circulation brings high-salinity water from the northwestern Arabian Sea (Han and McCreary, 2001; Rao and Sivakumar, 2003). The SSS is freshest during boreal fall in the Pacific and Atlantic ITCZ; there, the minimum SSS occurs 2–3 months after maximum P and maximum eastward flow of the North Equatorial Counter Current (NECC), which brings low salinity waters from the west (Delcroix and Hénin, 1991; Dessier and Donguy, 1994; Reverdin et al., 1994b; Arnault, 1987). This 2–3 month time lag is consistent with the change in SSS ($\partial S/\partial t$) being related to E−P and zonal salt advection (for details, see Hires and Montgomery, 1972). It is noteworthy that the timing of the mean seasonal SSS cycle is not quite uniform from track

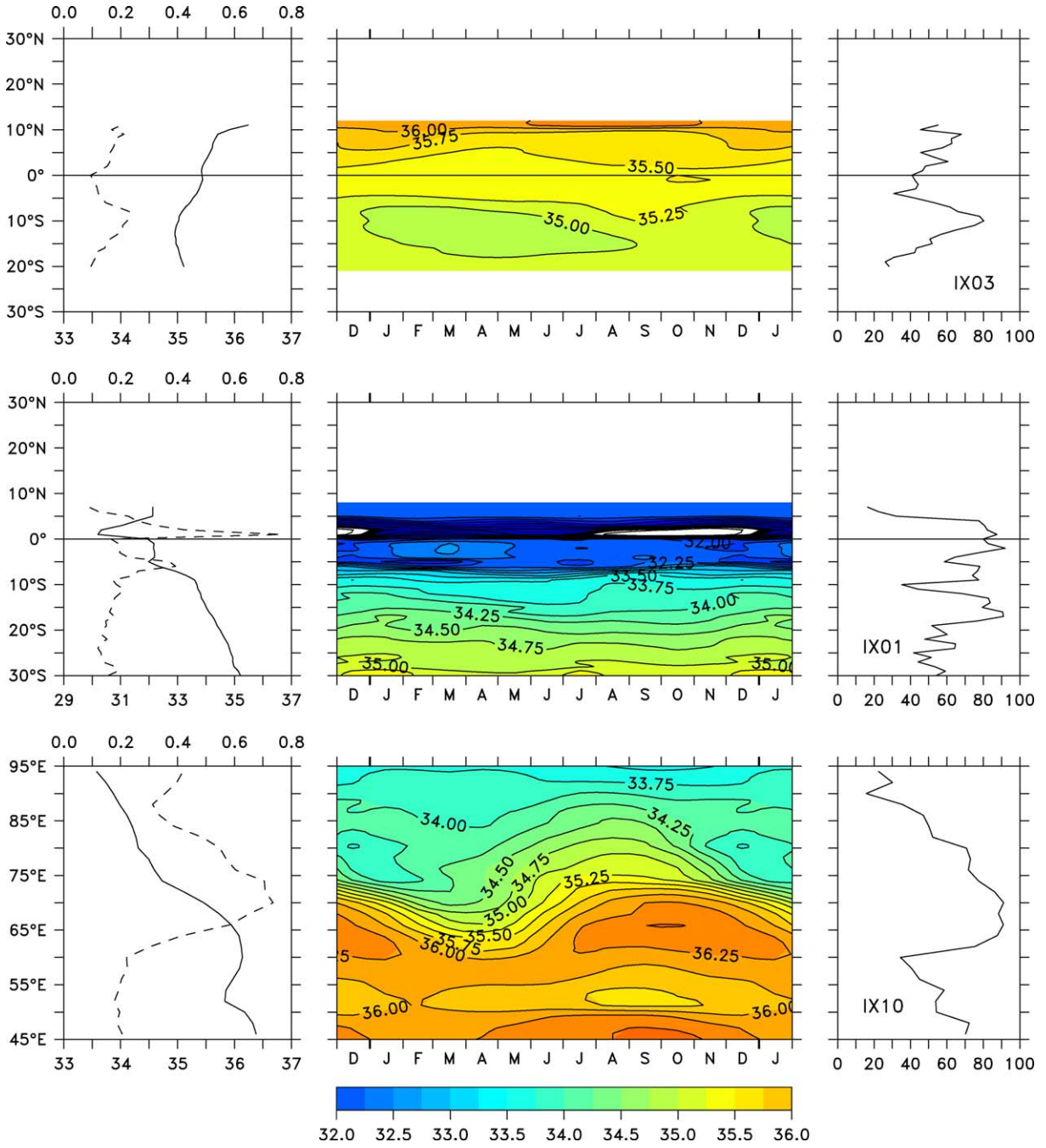

Fig. 3. Characteristics of sea surface salinity measured in the Indian Ocean along the two quasi-NS-oriented (top panels) IX03 and (middle panels) IX01 shipping lines, and the quasi-EW-oriented (bottom panels) IX10 shipping line. The left panels present the mean (full lines, bottom scales) and standard deviation (dashed lines, upper scales) values; the middle panels present the mean seasonal cycle based on monthly averages (contour intervals are 0.25 and the color code is shown at the very bottom); and the right panels present the percentage of variance in monthly averaged time series explained by the mean seasonal cycle. Note that vertical scales denote either latitudes or longitude, and the different horizontal scales on the left panels.

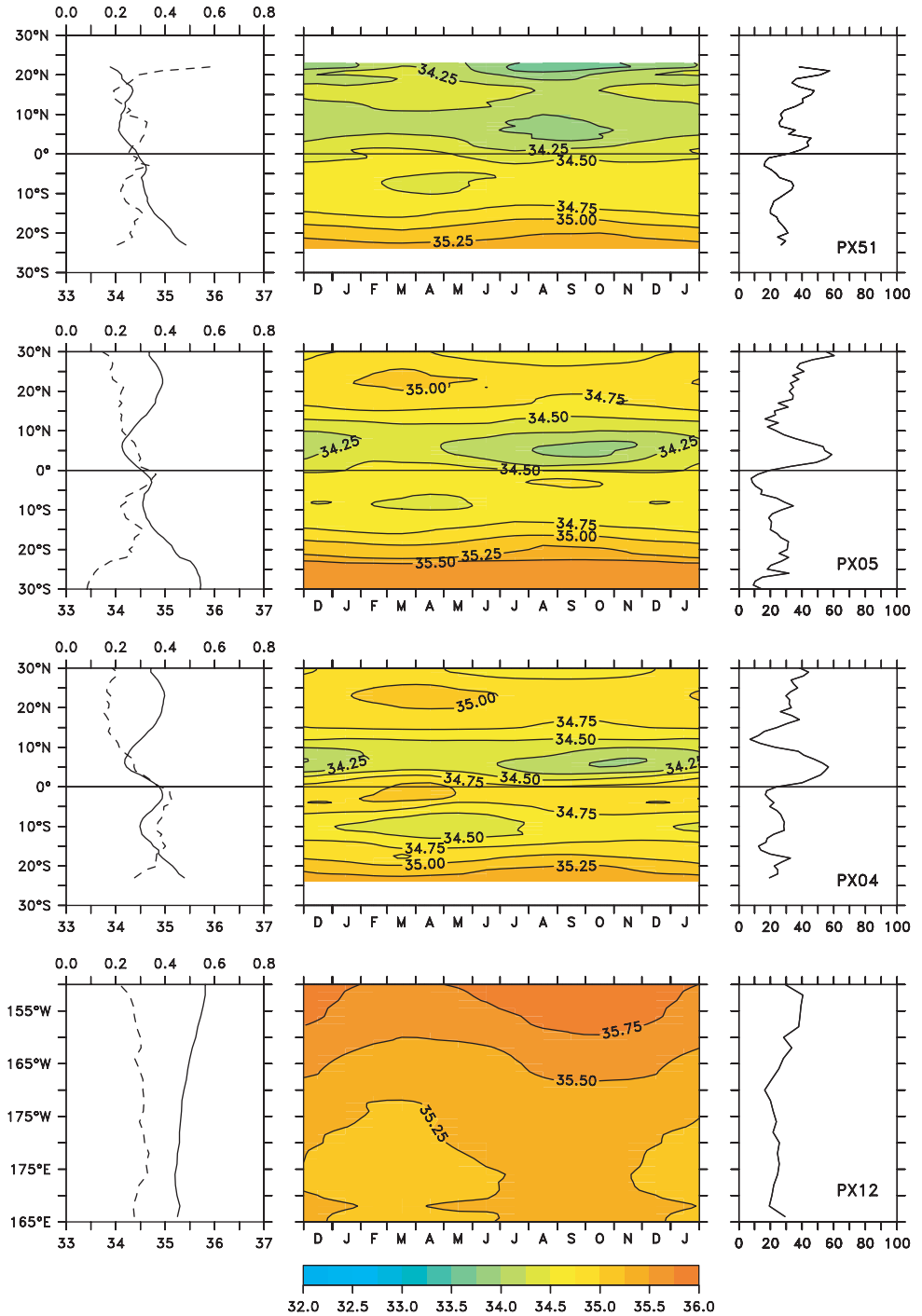

Fig. 4. Same as Fig. 3 for sea surface salinity measured in the western half of the tropical Pacific. From top to bottom panels are lines PX51, PX05, PX04 and PX12.

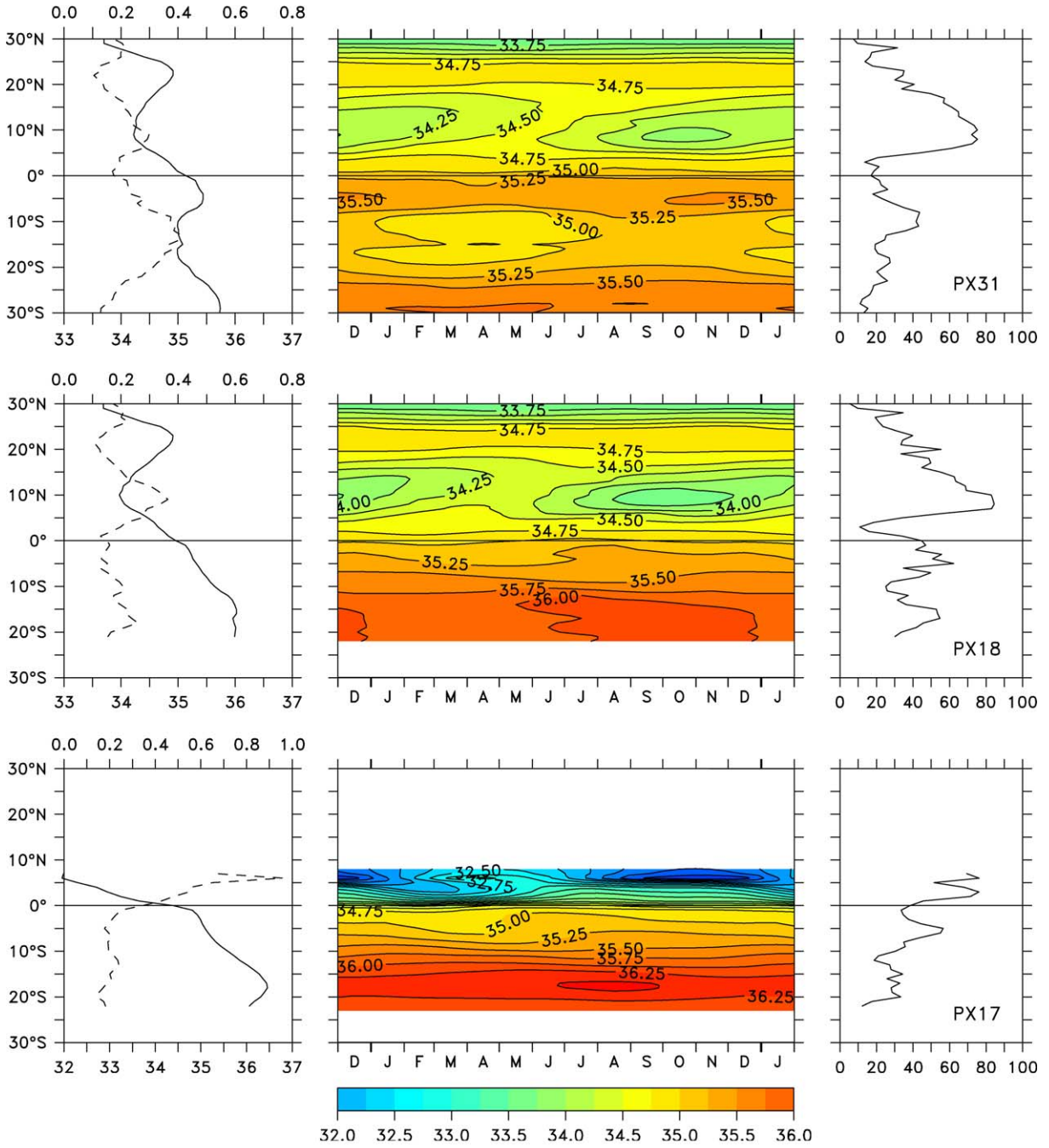

Fig. 5. Same as Fig. 3 for sea surface salinity measured in the eastern half of the tropical Pacific. From top to bottom panels are lines PX31, PX18 and PX17.

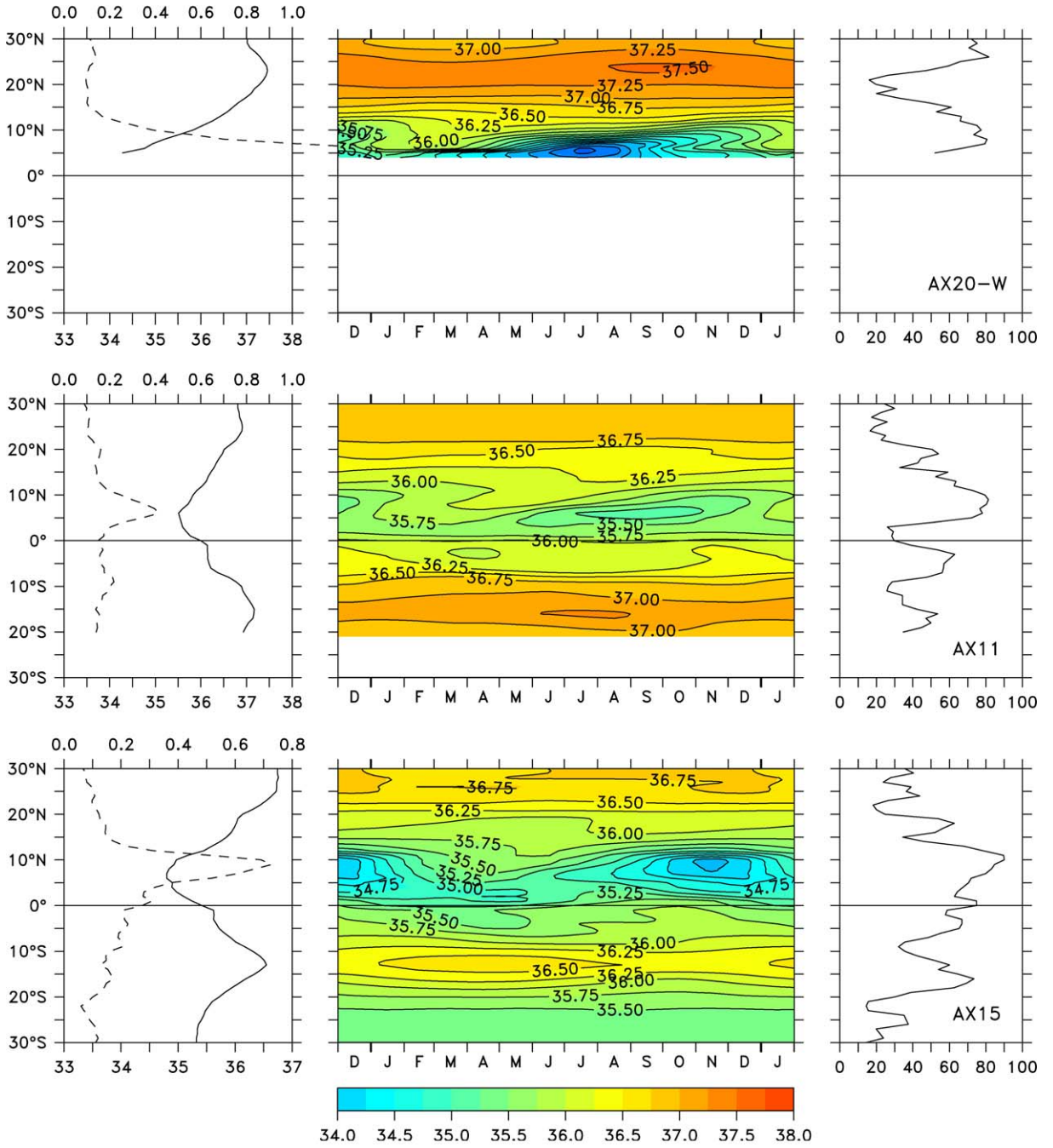

Fig. 6. Same as Fig. 3 for sea surface salinity measured in the tropical Atlantic. From top to bottom panels are lines AX20-W, AX11 and AX15.

to track in the western Pacific (tracks PX51, PX05, PX04) and Atlantic (AX20-W, AX11, AX15) oceans where the minimum SSS appears gradually later in the year from the west to the east. This is likely due to the heavy P associated with the E–NE/W–SW tilted ITCZ which, when moving equatorward in boreal fall, first affects the westernmost regions. Advection of relatively fresh water from the west by the NECC may also affect this phasing.

4. Time and space scales and signal to noise ratio for SSS

Monthly time series of SSS are available on 11 quasi-NS- and two quasi-EW-oriented VOS lines (with 1° latitude and 2° longitude resolutions), as well as on 35 TAO/TRITON and 13 PIRATA moorings (with 2–4° latitude and 3–15° longitude resolutions). These gridded fields enable us to estimate decorrelation scales and signal to noise ratios. Decorrelation scales indicate the distance in longitude, latitude or time over which SSS variations become decorrelated or, in other words, the typical size of coherent SSS features. The signal to noise ratio represents a normalized value of the expected signal resulting from a given sampling strategy; it is greater than one when the variability inferred from that strategy exceeds the unresolved variability.

4.1. Statistical methods

To estimate the decorrelation scales, mean values and temporal trends were first removed to produce SSS anomalies. For the 11 quasi-NS-oriented ship tracks, the along-track autocorrelation functions (hereafter referred to as ACF) were then estimated at each degree latitude by correlating time series at that latitude with all other time series at lags in latitude. An example of such lagged correlations is shown in Fig. 7a for the PX05 track using the equatorial 1970–2001 SSS time series as a reference. For each latitude, the smaller of the correlation values computed to either the north or the south were then selected to define the meridional ACF. Values of the ACF near the northern and southern tips of each track may thus be biased, as they are computed from fewer data. Examples of the resulting 61 (every degree latitude from 30°N to 30°S) ACF of the PX05 track are shown in Fig. 7b. The meridional decorrelation scales "Y" were then defined as the e-folding scale of fitted Gaussian curve $A(y) = -\exp(y^2/Y^2)$ as exemplified in Fig. 7c. A Gaussian was found to best resemble the shape of the ACF, as compared to half a dozen of other possible analytical formulas (see Denman and Freeland, 1985). Similar calculations were performed for the two quasi-EW-oriented ship tracks to estimate the zonal decorrelation scales, and in the time domain for all tracks to estimate the temporal decorrelation scales.

As was done with the VOS data, monthly SSS time series from the TAO/TRITON and PIRATA moorings were used to estimate the temporal decorrelation scales at fixed points. In the space domain, unlike the VOS, a full set of regular spatial lags cannot be obtained from the mooring arrays given their 2–4° latitude and 3–15° longitude resolutions. Two approaches were thus adopted to extract as much information as possible on spatial scales. First, for meridional scales, we systematically checked that the limited sets of correlations derived from the moorings gave results that were consistent with those derived from nearby ship tracks as exemplified in Fig. 7a. Second, for zonal scales, we used all possible pairs of locations at a given latitude with at least 2 years of simultaneous observations so as to compute cross-correlations of SSS time series for various space lags, and then derived zonal scales via curve fitting. This last technique is admittedly rather crude as the cross-correlations represent different time periods and record lengths. However, as discussed below, it provides information consistent with that obtained from the VOS lines.

The signal to noise (S/N) ratio squared was computed by projecting the estimated ACF from the value in the first bin into the origin (Gandin, 1963; Meyers et al., 1991). Given the estimated value at the origin μ_0, the ratio α^2 was defined as $\mu_0/(1-\mu_0)$. The signal to noise ratios could be computed from the value of μ_0 derived from either

the zonal (for EW-oriented ship tracks), meridional (for NS-oriented ship tracks) or temporal (for all ship tracks and moorings) ACF. For all ship tracks, the spatial ratios were found to be 0–25% greater than the temporal ratios. Hence, the ratios presented below were estimated from the *temporal* ACF which can be computed and compared for NS and EW ship tracks and moorings, and represent the more conservative values.

4.2. Results

Values of the meridional, temporal, and zonal scales, as well as the S/N ratios, for all ship tracks are shown in Figs. 8–14. Also shown are the corresponding values derived from nearby moorings whenever possible. The meridional scales are similar for the western Indian Ocean (track IX03), the eastern half of the Pacific Ocean (tracks PX31, PX18, PX17), and the Atlantic Ocean (tracks AX20-W, AX11, AX15) with values of the order of 2–3° latitude (except south of 10°S along IX03 where they reach 5° latitude). In the western Pacific warm pool (tracks PX51, PX05, PX04), the meridional scales are generally higher, increasing on average from about 4° latitude in the equatorial band to 7° latitude towards 20°N and 20°S.

The temporal scales are also similar for most tracks, with values of about 2–3 months reflecting the prominence of the mean seasonal cycle. An exception to this is found in the Pacific warm pool region where the temporal scales increase from about 2 months at 20°N to 6 months at 20°S. There is an interesting relative extremum of 5–6 months located slightly south of the equator (tracks PX05, PX04; Fig. 9) where the ENSO signature in SSS is maximum (Delcroix and Hénin, 1991; Delcroix and McPhaden, 2002). A temporal scale of 5–6 months is also found in the SPCZ

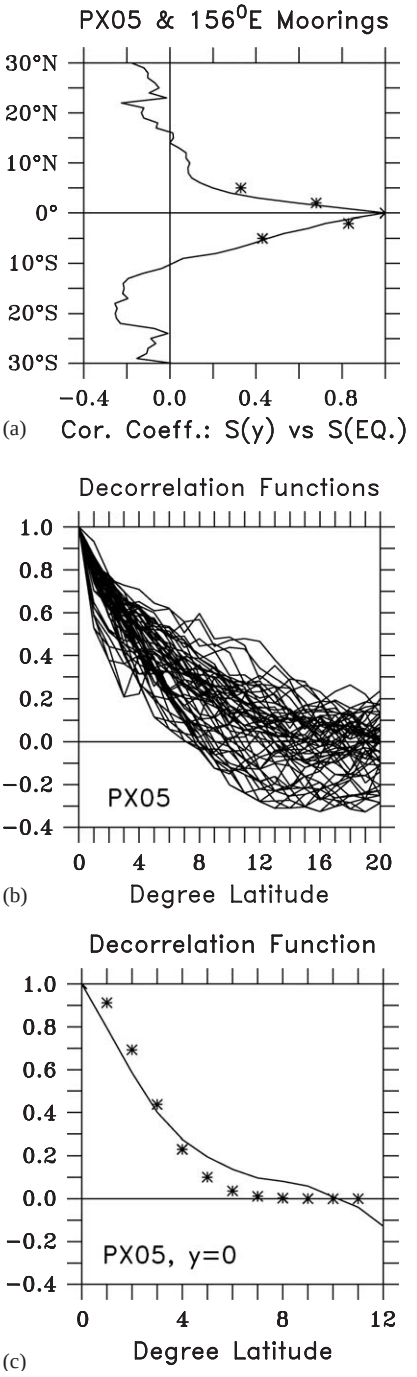

Fig. 7. (top) Meridional variations of the correlation coefficients between SSS time series at the equator versus SSS time series at all other latitudes. The full line is for the PX05 track, and the stars denote the limited set of correlations provided by the 2–5° latitude resolution of the 156°E TAO/TRITON moorings. (middle) Meridional decorrelation functions plotted for each latitude, from 30°N to 30°S, of the PX05 track. (bottom) The full line is the observed decorrelation function at the equator for the PX05 track and the stars are the corresponding least-squared fitted Gaussian function. In this particular case, the meridional decorrelation scale equals 3.6° latitude and the meridional signal to noise ratio equals 2.0.

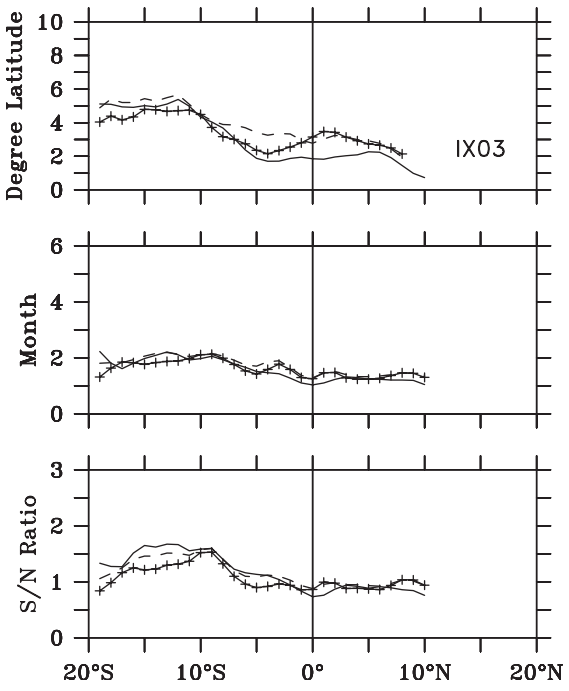

Fig. 8. From top to bottom: meridional scales, temporal scales, and signal to noise ratio estimated for the IX03 shipping line, for 1977–1986 (full lines), 1987–1996 (full lines with crosses), and 1977–1996 (dashed lines).

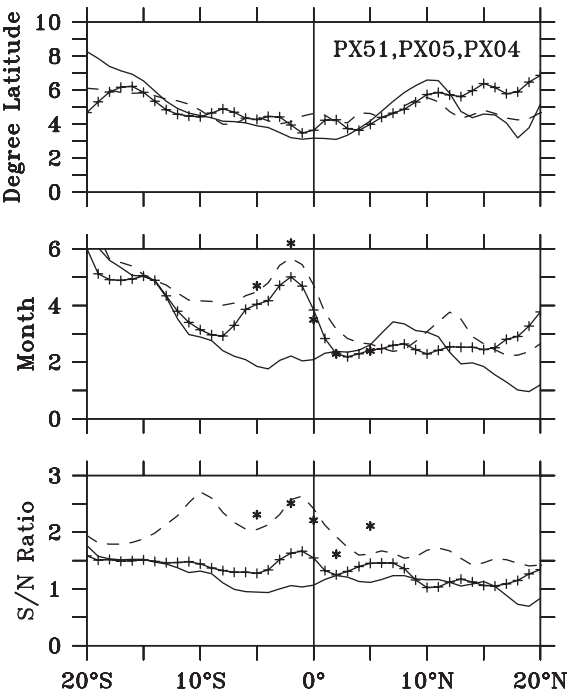

Fig. 9. From top to bottom: meridional scales, temporal scales, and signal to noise ratio estimated for the PX51(full lines), PX05 (full lines with crosses), and PX04 (dashed lines) shipping lines. The stars denote the corresponding values estimated from the nearby 156°E TAO/TRITON mooring sites.

region (track PX12; Fig. 13) where ENSO time scales dominate the SSS record (Gouriou and Delcroix, 2002).

Computation of zonal scales can be derived for two ship tracks only, one in the Indian Ocean (IX10) and the other in the Pacific SPCZ (PX12). Along IX10, the zonal scale ranges from 6–7° longitude south of India to 3° longitude towards the Malacca Strait and the Gulf of Aden. It is much larger and of the order of 15–20° longitude along PX12 in the Pacific SPCZ. The 19 possible cross correlations computed from the moored time series data from equatorial sites in the Pacific are shown in Fig. 15 where the e-folding scale of the Gaussian fit (i.e., the zonal decorrelation scale) equals 17.4° longitude. At 2°N in the Pacific, the Gaussian fit to the nine possible cross correlations gives a zonal decorrelation scale of 17.6° longitude, a value that is the same order of magnitude as those obtained in the SPCZ and along the equator. Regardless of which mooring is used as a reference, there is no clear evidence of an E–W variation in this zonal scale (Fig. 15), though the relatively small number of cross correlations on which these results are based leaves some ambiguity as to the robustness of this conclusion. Computation of zonal decorrelation scales at other latitudes in the Pacific or in the Atlantic is not possible because of the inadequate number of simultaneous SSS time series in longitude.

Sensitivity studies were performed to determine the effects of choosing different time periods for computing decorrelation scales and S/N ratios. These were done by using 5–20 year moving windows for the Indian and Atlantic tracks, and in using either the El Niño (SOI <0) or La Niña (SOI >0) only periods for the Pacific tracks. Nearly identical values are obtained for the meridional and temporal scales and S/N ratio computed for the western Indian Ocean (track

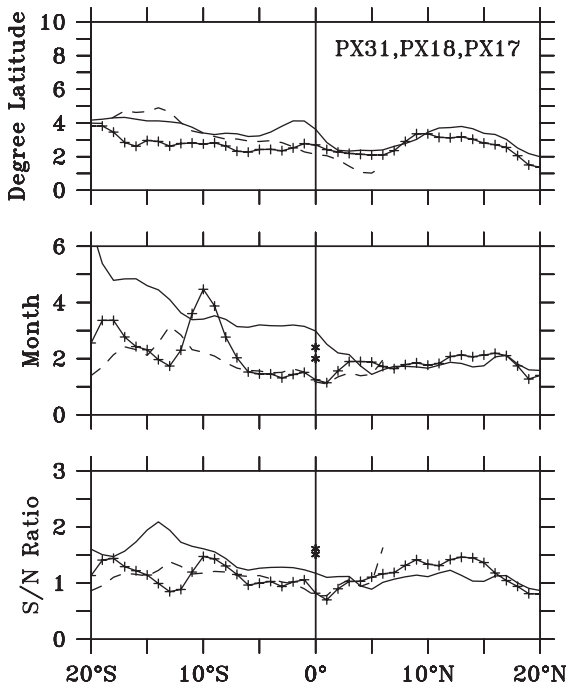

Fig. 10. From top to bottom: meridional scales, temporal scales, and signal to noise ratio estimated for the PX31 (full lines), PX18 (full lines with crosses), and PX17 (dashed lines) shipping lines. The stars denote the corresponding values estimated from the nearby equatorial 125°W and 110°W TAO/TRITON mooring sites.

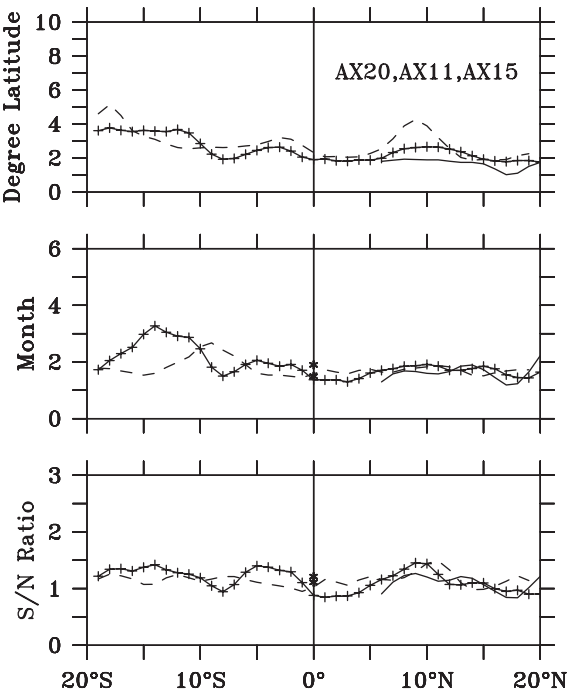

Fig. 11. From top to bottom: meridional scales, temporal scales, and signal to noise ratio estimated for the AX20-W (full lines), AX11 (full lines with crosses), and AX15 (dashed lines) shipping lines. The stars denote the corresponding values estimated from the nearby equatorial 35°W and 10°W PIRATA mooring sites.

IX03) for two 10-year (1977–86; 1987–96) periods and a 20-year (1977–96) period (Fig. 8). Similar tests confirm that the analyzed values for the Indian and Atlantic tracks are only weakly sensitive to the chosen time period, as long as at least one decade of data is available (i.e., with the exception of track IX01). In contrast, the magnitude of zonal, meridional and temporal scales changes depending on the sign of the Southern Oscillation Index (SOI) for the tracks crossing the warm pool. For PX05 (Fig. 14), which has the longest time series, the meridional scale for La Niña is about 60–80% of those for El Niño within 10°N–10°S, and the temporal scale is about 50% within 0–5°S. (Note that lagging the SSS time series by 2–3 months relative to the SOI to account for the phased development of observed features during ENSO events did not change these percentages significantly.) Other changes were found barely significant. To summarize, SSS decorrelation scales in the western tropical Pacific tend to be smaller during La Niña time periods, with values approaching those found for the central Pacific in Fig. 10, consistent with the fact that warm pool waters are pushed farther to the west during La Niña.

The ratios of zonal to meridional or temporal scales are of interest regarding the choice of bin sizes when gridding irregularly distributed observations. Based on our results, it appears that there is a 1/5 latitude/longitude aspect ratio for SSS variability on monthly time scales, a result that is fairly consistent with the choices made by previous above-noted investigators analyzing SSS changes in the tropics. Variations in these ratios do exist however, for example in the western Arabian Sea where the zonal and meridional scales are of the same order.

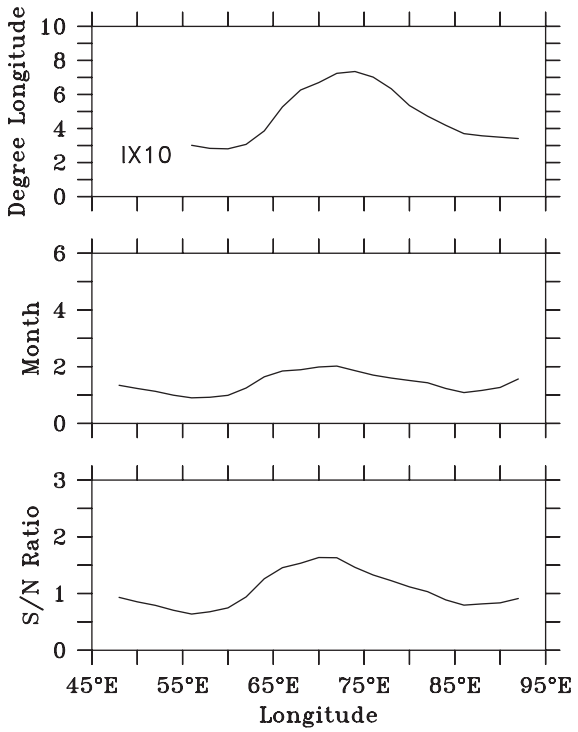

Fig. 12. From top to bottom: zonal scales, temporal scales, and signal to noise ratio estimated for the IX10 shipping line.

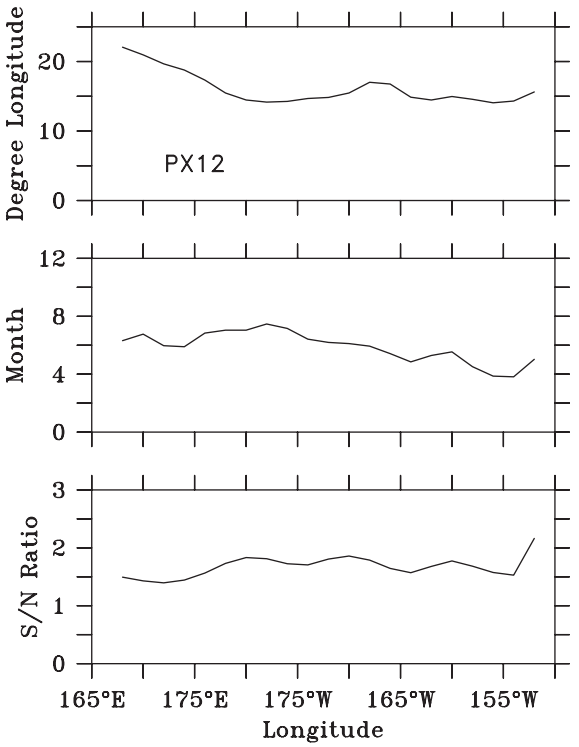

Fig. 13. From top to bottom: zonal scales, temporal scales, and signal to noise ratio estimated for the PX12 shipping line.

The S/N ratios are overall on the order of 1–1.5. They are somewhat higher near the eastern edge of the western Pacific warm pool (see track PX04 and TAO/TRITON moorings) as expected since temporal variations are dominated by ENSO-related EW migration of the zonal SSS front (Picaut et al., 2001). The S/N ratio is only slightly above unity, however, indicating that there is part of the SSS variability that is not resolved with our gridding procedure. This small-scale variability is discussed in the following section.

5. Sampling and averaging issues

Because of the relative sparseness of SSS observations and the need to rely in part on interpolation techniques, our scale and S/N estimates were based on gridded fields with bin sizes of 2° longitude, 1° latitude and 1 month. Variability on scales smaller than these bin sizes is not resolved. Hence, this section takes advantage of the high-resolution VOS- and mooring-derived TSG observations to characterize this variability, and then to discuss sampling and averaging errors resulting from past, present and future observation systems. The sampling error is defined below as the ability of a unique measurement within a given interval to represent the true mean over that interval. Similarly, the averaging error is defined as the ability of a given number of measurements within a given interval to represent the true mean over that interval.

5.1. Illustration of small-scale SSS variability

To illustrate the small-scale time variability at one location, Fig. 16 shows the longest (1988–2002) daily SSS time series collected at the 0–165°E TAO/TRITON mooring, together with the standard deviations of SSS over 10 and 30

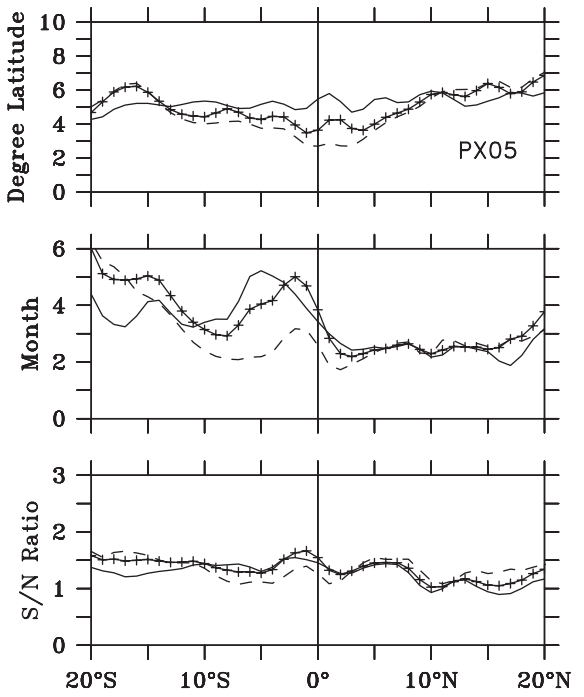

Fig. 14. From top to bottom: meridional scales, temporal scales, and signal to noise ratio estimated for the PX05 shipping line. The estimates were made by considering SSS values at times of negative SOI (El Niño conditions; full lines), at times of positive SOI (La Niña conditions; dashed lines), and at all times regardless of the SOI phase (full lines with crosses).

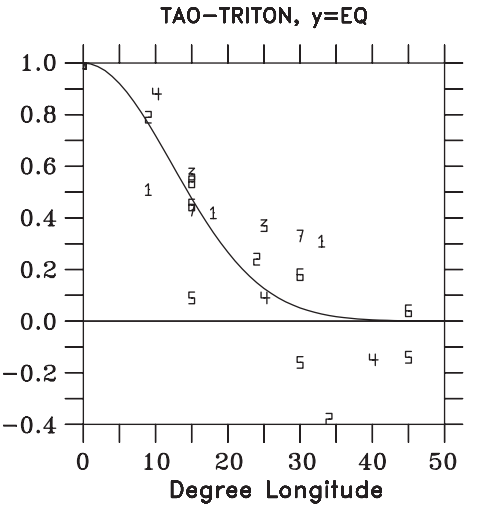

Fig. 15. Correlation coefficients between monthly SSS time series derived from a reference equatorial mooring in the Pacific versus SSS time series derived from other equatorial moorings at lags in longitude. The numbers on the plot denote the reference moorings, from number 0 at 137°E to number 9 at 110°W (see Table 2). The full line is the least-squared fitted Gaussian function.

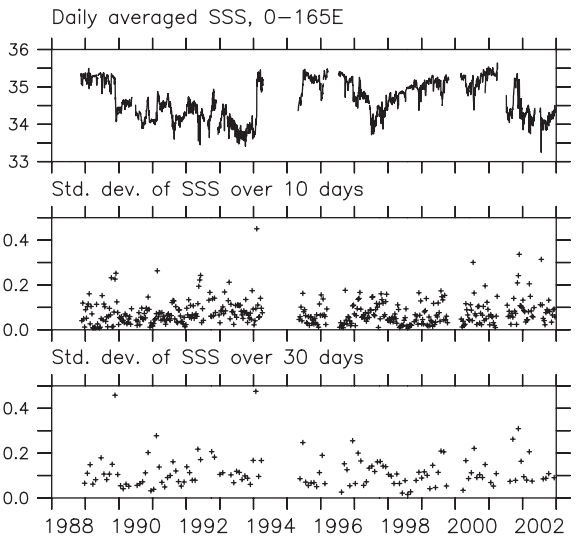

Fig. 16. Daily SSS changes recorded at the 0–165°E TAO/TRITON mooring, and standard deviations of SSS computed over 10- and 30-day intervals.

days. The 10-day period is chosen to correspond closely to future nominal satellite sampling intervals, and the 30-day period corresponds to monthly averages used in studies of seasonal-to-interannual variability. Aside from the discernible ENSO signal (e.g., Delcroix and McPhaden, 2002), Fig. 16 further indicates that there are small time scale SSS changes that are not negligible. Indeed, although most 10- and 30-day standard deviations are less than 0.2, i.e. less than 50% of the long-term variability shown in Fig. 4, there are a few instances when they clearly exceed 0.2. The most spectacular case occurs in early 1994 (see also Delcroix and McPhaden, 2002, their Fig. 3) when the standard deviations are near 0.5. Such high values occur at times when the zonal SSS front located at the eastern edge of the warm pool crossed 0–165°E while moving eastward (westward) during El Niño (La Niña) events (see Picaut et al., 2001).

A similar approach illustrates the small-scale meridional variability along a quasi-NS-oriented

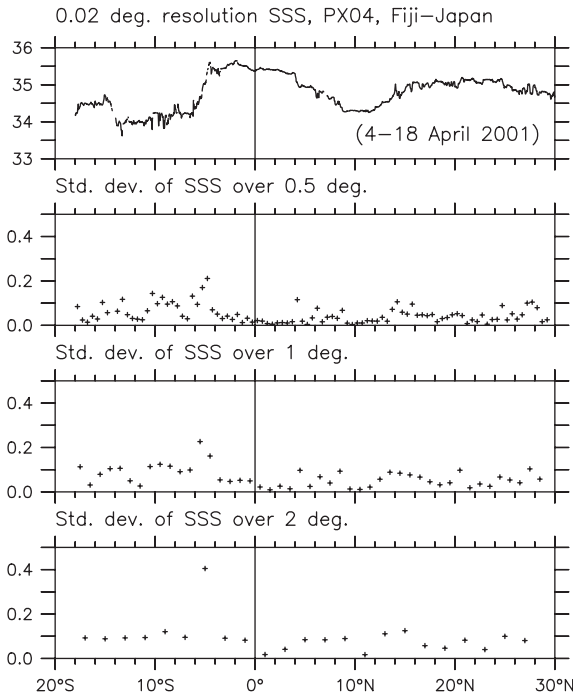

Fig. 17. High-resolution SSS observations recorded along the Fiji–Japan shipping track (PX04) during 4–18 April 2001, and standard deviations of SSS computed over 0.5°, 1° and 2° latitudes.

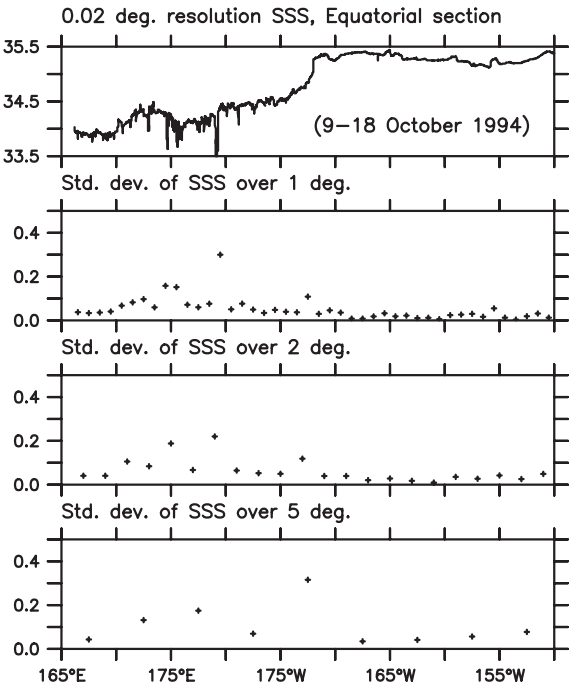

Fig. 18. High-resolution SSS observations recorded along the equator during 9–18 October 1994, and standard deviations of SSS computed over 0.5°, 1° and 2° longitudes.

ship track. Fig. 17 shows the 0.02° resolution SSS measurements collected in April 2001 in the western Pacific warm pool (track PX04), together with the standard deviations of SSS over 0.5°, 1° and 2° latitude intervals. These intervals represent the likely distance over which future satellite measurements will be averaged, and they are the most common meridional bins used in observational and general circulation numerical model studies. The three bottom panels of Fig. 17 show that the standard deviations are generally less than or equal to 0.1 which are relatively small compared to the long-term variability along this track (Fig. 4). Again, however, there are some instances where the standard deviations amount to as much as 0.2–0.4, especially near the meridional SSS front marking the southern part (4–6°S) of the equatorial upwelling zone where variability is unusually strong during this La Nina time period.

A final illustration of small-scale zonal variability is given in Fig. 18 from the 0.02° resolution SSS measurements collected during a research cruise carried out along the equator within 165°E–150°W in October 1994 (Eldin et al., 1997). The standard deviations computed over 1°, 2° and 5° longitude intervals are mostly less than or equal to 0.1, with however notable values in excess of 0.2–0.3. These high values happen in particular in the western half of the equatorial section (see the "noisy" SSS curve west of about 175°W), where heavy local precipitation associated with SST above 29.5°C resulted in small-scale SSS changes. Also, the occurrence of a sharp zonal front near 172°W resulted in a standard deviation computed over 5° longitude greater than 0.3 between 170°W and 175°W. Such a zonal front is not unusual at the eastern edge of the warm pool (e.g., Kuroda and McPhaden, 1993; Picaut et al., 2001; Kobayashi and Takahashi, 2002) and, given the climatic importance of this front, its variability

should be considered in developing future sampling strategies.

5.2. Sampling issues

The top panels in Figs. 16–18 indicate that small-scale SSS changes could induce large errors when a single observation is taken within a given interval as representing the true mean over that interval. We showed that this is especially relevant in the warm pool where one can find rapid temporal (Cronin and McPhaden, 1998), meridional (Hénin and Grelet, 1996), or zonal (Eldin et al., 1997) changes. Lagerloef and Delcroix (2001) discussed the sampling errors for similar examples by computing the standard deviations of 10-day samples in mooring time series and of 2°-samples in the ship transects. They showed that the sampling error is generally less than 0.1, though it can sometimes approach 0.3 in the presence of unusually strong SSS gradients. Thus, we cannot exclude the possibility that such errors might have biased published work including some of those by the present authors. This could especially be the case when the results were derived from gridded fields obtained from low time–space resolution data provided by bucket samples, which constituted the main observational technique before the 1990s. On the other hand, temporal aliasing of moored buoy SSS data and aliasing in the along track direction of the most recent VOS observations should be minimal since these are much higher-resolution data.

5.3. Averaging issues

The high-resolution data in time (from moorings) and in latitude/longitude (from VOS) measurements are now used to discuss averaging errors. We specifically want to address the question of what is the minimal number of measurements over a given interval that are needed to obtain a mean value with a specified accuracy. For this purpose, the Global Ocean Data Assimilation Experiment (GODAE) requirements of 0.1 for accuracy, 10 days for temporal resolution and 1° latitude and 2° longitude for horizontal resolution are used as a reference.

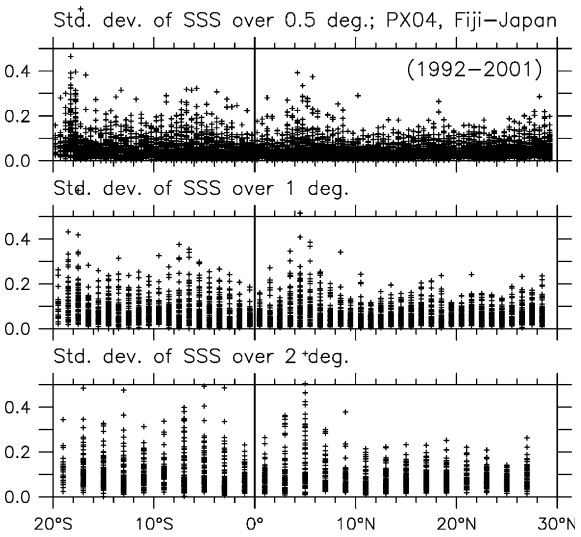

Fig. 19. Distribution of the standard deviation values of SSS computed over 0.5°, 1° and 2° latitudes for all 1992–2001 voyages along the Fiji–Japan shipping track (PX04).

The three bottom panels in Fig. 17 show the standard deviations of SSS computed over 0.5°, 1° and 2° latitude for the typical 4–18 April 2001 voyage along the PX04 track. A similar figure for all the 1992–2001 voyages along PX04 is presented in Fig. 19 to more precisely quantify the expected variability over these latitude intervals. It is evident that the highest values shown in Fig. 17 are not unusual, especially around the 5°N and 5°S latitudes which roughly delimit the meridional extent of the equatorial upwelling. Fig. 20 further presents the frequency distribution of SSS standard deviations in 0.02 bins for the 0.5°, 1° and 2° latitude intervals. This distribution is computed for all latitudes, but a similar plot would hold for any given latitude. Results indicate that the distribution of SSS variability exhibits positive skewness, with an asymmetric tail extending towards higher values. We can summarize the information in Fig. 19 by computing and plotting the mean values of the standard deviations for each interval as a function of latitude. These plots are presented in Figs. 21 and 22 for all quasi-EW and NS-oriented ship tracks. Similarly, mean values of SSS standard deviations are computed

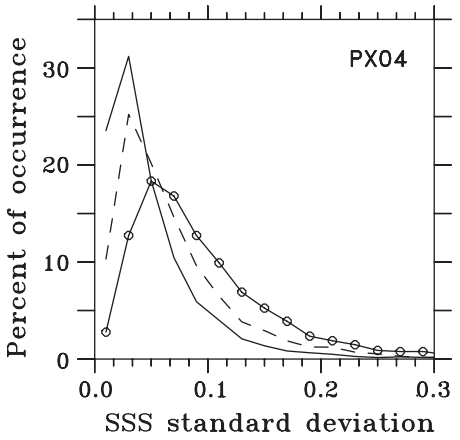

Fig. 20. Percent of occurrence of SSS standard deviation values in 0.02 bins computed over (full line) 0.5° latitude, (dashed line) 1° latitude, and (full line with circles) 2° latitude for all 1992–2001 voyages along the Fiji–Japan shipping track (PX04).

over 10- and 30-day intervals for each Pacific and Atlantic mooring site having at least 2 years of data (Table 2).

Overall, the mean standard deviations over 0.5°, 1°, and 2° latitude are respectively 0.07, 0.10, and 0.14 (Fig. 21). Also, from the two EW ship tracks, the mean standard deviations over 1°, 2°, and 5° longitude are respectively 0.08, 0.12, and 0.19 (Fig. 22). Based on the values in Table 2, the mean standard deviations over 10 and 30 days are 0.10 and 0.15, respectively. So, by using 0.10 as the mean standard deviation computed over 1° latitude, 0.12 as the mean standard deviation computed over 2° longitude, and 0.10 as the mean standard deviation computed over 10 days, the root sum square in all three dimensions (x, y, t) combined gives $\sigma = (0.10^2 + 0.12^2 + 0.10^2)^{1/2}$ or 0.185. This result indicates that the *mean* expected SSS variability within a box of 1° latitude, 2° longitude and 10 days for the regions examined is of the order of 0.2. Hence, taking the GODAE resolution and accuracy requirements for SSS as a reference, if one wishes to determine SSS with an accuracy of $a = 0.1$ over 10 days, 1° latitude and 2° longitude, the minimum number of measurements, as given by $N = 4\sigma^2/a^2$ (see Emery and Thomson, 1998; p. 224), is $N = 14$ observations. A similar calculation shows that the

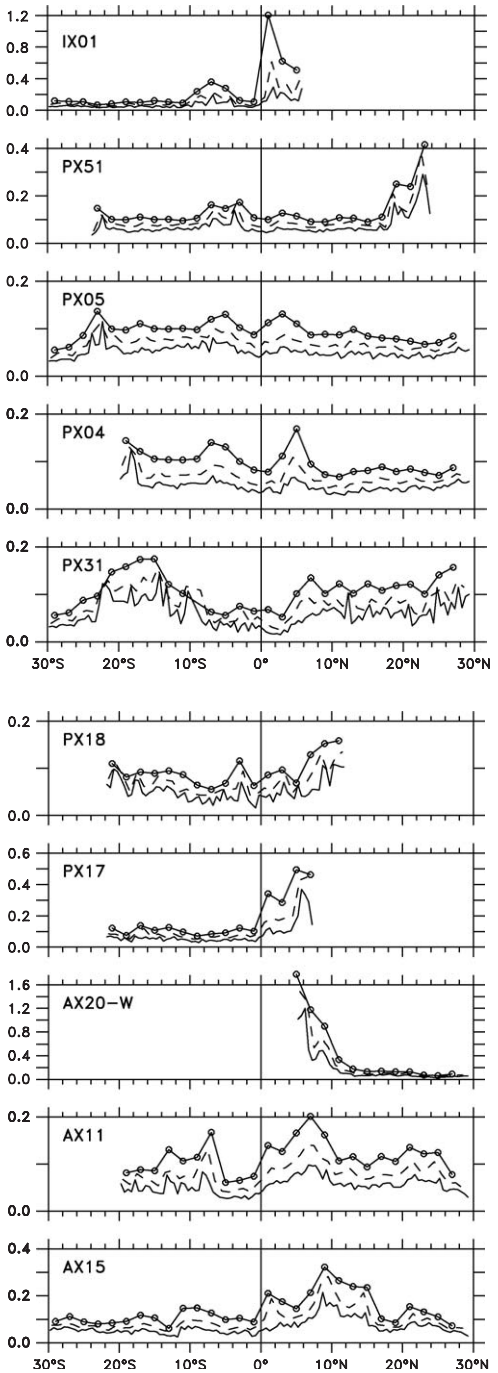

Fig. 21. Mean values of the standard deviations of SSS computed over (full lines) 0.5° latitude, (dashed lines) 1° latitude, and (full lines with circles) 2° latitude. Note the different vertical scales depending on the signal amplitude on each ship track.

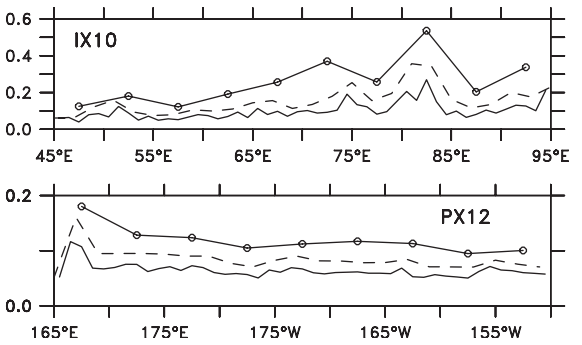

Fig. 22. Mean values of the standard deviations of SSS computed over (full lines) 1° longitude, (dashed lines) 2° longitude, and (full lines with circles) 5° longitude. Note the different horizontal and vertical scales, depending on the signal amplitude and on the ship track.

minimum number of observations becomes $N = 4$ if one wishes to determine SSS with an accuracy $a = 0.2$ (instead of 0.1) over the same box.

The above calculation assumes that SSS is normally distributed, which as discussed by Bingham et al. (2002) is not strictly valid for most regions. It also assumes the N observations to be independent, which requires an estimate of decorrelation scales for the small scale SSS "noise" variability. These decorrelation scales are obviously not homogeneous in time and space, as can be intuited in Fig. 18 by comparing the small scale SSS variability east and west of 175°W. We believe however that it is instructive to determine the possible range of values, and so we estimated the decorrelation scales for each mooring site and ship track from the high-passed (in time, latitude, and longitude) SSS data. At each mooring site, we computed SSS variations at periods equal to or shorter than 10 days (30 days) as residuals between 21 days (61 days) Hanning filtered time series and the original SSS time series. Similarly, we computed SSS variations at periods equal to or shorter than 1° and 2° latitude for each NS-oriented shipping track, and at periods equal to or shorter than 2° and 5° longitude for each EW-oriented shipping track. The decorrelation scales are 2.3 ± 0.6 (5.2 ± 2.3) days on time scales less than 10 (30) days, $0.23 \pm 0.06°$ ($0.42 \pm 0.10°$) latitude on meridional scales less than 1° (2°) latitude, and $0.43 \pm 0.12°$ ($0.81 \pm 0.32°$) longitude on zonal scales less than 2° (5°) longitude. (The first number is the mean and the second number is the standard deviation.) These numbers indicate that, on average, we can obtain about 4 (6) independent samples in a 10 (30)-day period for the moorings, 4 (5) independent samples over 1° (2°) latitude for the NS transects, and 5 (6) independent samples over 2° (5°) longitude for the EW transects. Hence, it appears that for the present SSS observing system, an accuracy of only about 0.2 (with $N = 4$) is achievable over large regions of the tropics at a resolution of 10 days, 1° latitude and 2° longitude. Higher accuracy can be expected in regions where we can obtain more than four independent samples by combining VOS and mooring measurements.

As a cautionary note, we should keep in mind that the two numbers σ and N discussed above were obtained in using the *mean* standard deviations computed over 1° and 2° latitude, 2° and 5° longitude and 10 and 30 days. Figs. 21 and 22, as well as Table 2, tell us that such values are highly variable in space and time and in particular can be much larger both in open ocean regions of strong SSS gradients and near coasts or off river mouths (e.g., north of the equator in IX01 and PX17, south of 10°N in AX20-W). In these latter cases, our results are not strictly applicable. Also, our conclusions regarding sampling requirements would change if resolution and accuracy requirements other than those recommended by GODAE were considered. Moreover, there remain vast regions in the tropics that are still not documented at all in terms of small-scale SSS variability. Hence, we expect that the analysis of SSS observations provided by the future dedicated satellite missions will be of great value in refining and expanding upon our conclusions.

6. Summary and conclusions

The goal of this work was first to provide an overview of SSS variability in the tropical oceans in order to improve our knowledge of that variability as well as to prepare for validating and analyzing future SSS measurements by remote

sensing. We have gathered an unprecedented collection of in situ observations collected from VOS, mooring and STD/CTD data during the 1970–2003 period. Comprehensive quality control procedures and examination of time/space distributions of the data lead us to restrict our study to SSS data obtained along 13 well-sampled ship tracks and at 35 TAO/TRITON and 13 PIRATA moorings (Fig. 2; Tables 1 and 2). The SSS variability was then analyzed from both gridded fields with bin sizes of 2° longitude, 1° latitude and/or 1 month, and from higher-resolution VOS and mooring-derived SSS records. In general, results based on shipboard and mooring data were consistent, and the availability of both kinds of data allowed for more in depth analysis of time and space scales of variability.

The SSS variability estimated from gridded fields is summarized in Fig. 23a showing the standard deviation values of SSS computed along ship tracks having at least 12 years of data (except track IX01 in the eastern Indian Ocean). It shows

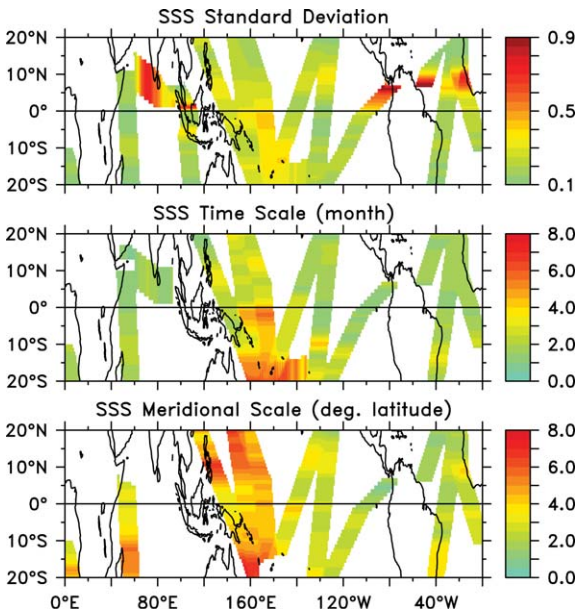

Fig. 23. Summary of SSS (top) standard deviations, (middle) time scales, and (bottom) meridional scales along the ship tracks shown in Fig. 2 and detailed in Table 1. The width of each track was arbitrarily chosen as 15° longitude or 10° latitude for clarity of the figure.

that monthly SSS variability lies generally within 0.1–0.3, with some notable exceptions. These can be found in: (a) the Atlantic ITCZ, in the eastern part of the Pacific ITCZ and along the track from Malaysia to the Gulf of Aden in the Indian Ocean (track IX10), where the seasonal cycle accounts for 60–90% of the observed variance, and (b) the western Pacific warm pool and in the SPCZ, where the ENSO variability dominates.

The gridded fields were further used to estimate the characteristic scales for SSS. The time and meridional scales are presented in summary form in Figs. 23b–c along the above noted ship tracks. (A summary figure for the SSS zonal scale is not given here as it could be estimated for three regions only.) In agreement with Fig. 23a, the SSS time scale (Fig. 23b) is generally less than 3 months in regions that have a strong seasonal cycle, whereas it ranges within 4–8 months where the variability is mostly controlled by ENSO. The SSS meridional scale (Fig. 23c) is about 2–3° latitude in the eastern half of the Pacific, in the Atlantic, and in the western equatorial Indian Oceans. Larger meridional scales appear: (a) in the western Pacific warm pool where SSS changes are mostly driven by zonal current and precipitation changes of similar scale, (b) poleward of 10° latitude in the western Pacific and southeastern Atlantic and (c) in the southwestern Indian ocean where the meridional surface circulation dominates over the zonal circulation. A SSS zonal scale of 15–20° longitude was found both in the equatorial Pacific, as derived from TAO/TRITON moorings (Fig. 15), and in the SPCZ, as derived from VOS (Fig. 13). A much smaller zonal scale of 3–7° longitude was found along about 8–10°N in the Indian Ocean (Fig. 12). Sensitivity tests indicate that the characteristic scales for SSS are altered in the western Pacific warm pool depending on the prevalence of El Niño or La Niña conditions. Such nonstationarity must be considered when gridding SSS data by means of objective analysis or when designing a monitoring network. The ratios of zonal to meridional and/or temporal scales are overall consistent with those determined in previous studies, although the differences we infer in latitude, longitude and temporal scales clearly indicate that uniform scales should not be

used for mapping SSS structures throughout the tropics.

Based on gridded fields, we also showed that the S/N ratios are on average of the order of 1–1.5, meaning that part of the SSS variability is not resolved when using bin sizes of 2° longitude, 1° latitude and 1 month are used. Daily records of SSS at mooring sites and 0.02° spatial resolution of TSG-derived SSS records along ship tracks were thus used to assess the short time/space variability and corresponding "noise" decorrelation scales. This variability was estimated by computing the standard deviation values of SSS over 10 and 30 days, over 0.5°, 1°, and 2° latitude, and over 1°, 2°, and 5° longitude (see Figs. 21 and 22 and Table 2). For example, the standard deviation of SSS over 30 days, as derived from TAO/TRITON moorings, is on the order of 0.15, a value which is 2–3 times larger than that derived from state-of-the-art models forced by daily air–sea fluxes (e.g., Wang and Chao, 2004). Also, we showed that the *mean* expected variability within a box corresponding to the GODAE resolution requirements for SSS (10 days, 1° latitude, and 2° longitude) is about 0.2, with values that can be much larger in specific regions. Based on this 0.2 mean value, we conclude that a minimum of 14 (4) independent observations are needed in such a box to meet a 0.1 (0.2) accuracy requirement. Computation of decorrelation scales based on the short time/space SSS noise variability enables us to approximate what constitutes an independent observation. For example, we estimated that, on average, it is possible to obtain four independent samples in a 10-day period, four independent samples in a 1° latitude band, and four independent samples in a 2° longitude band. Hence, at present, the existing observing system appears adequate to resolve SSS variability with an accuracy of 0.2 at a resolution of 10 days in time, 1° latitude, and 2° longitude. This accuracy is twice the GODAE requirement of 0.1. As can be seen from Fig. 2, we can expect that there are few regions at present in the tropics where both VOS and mooring data coexist to meet this GODAE requirement.

It is likely that the relative inability of models to reproduce observed SSS changes results in large part from the poor accuracy of air–sea fluxes, and in particular precipitation. Improved definition of SSS variability would be a valuable constraint on these fluxes (Vialard et al., 2002; Deltel et al., 2004), but we are not yet taking full advantage of the existing programs to enhance in situ SSS measurements. For example, east of the dateline in the Pacific there are relatively few TAO moorings presently instrumented with salinity sensors. Likewise, SSS observations are virtually nonexistent in the southeastern tropical Pacific and central Indian oceans where there is potential for recruiting new VOS ships. Finally, the results in this paper are based on the best collection of SSS data available at the present time. We believe that our analyses should be revisited and refined as more data are accumulated from in situ measurement programs and from well-calibrated and validated remotely sensed observations by remote sensing, especially in the vastly under-sampled regions that presently exist.

Acknowledgements

This paper is dedicated to the late L. Foucher from IRD-Nouméa. Compiling more than three decades of in situ SSS data is the result of the hard work and intellectual efforts of a large body of scientists, engineers, technicians, administration people, ship officers and crews within agencies and institutions. While we have no room to name them individually, we do acknowledge their long-lasting efforts. We also thank G. Reverdin who provided some validated VOS data in the tropical Atlantic and Y. Kuroda who provided the TRITON data in the western tropical Pacific. We also acknowledge the TAO Project Office of NOAA/PMEL for providing free and open access to TAO and PIRATA data through the World Wide Web. We appreciate the reviewer's comments which contributed to improvements in the paper. This work was supported by a grant from CNES, France, as preparatory works for future SMOS data availability (TD, YG), by a grant from Mercator, France, as preparatory works for real time SSS data assimilation in OGCM (TD, YG), and by NOAA's Office of Oceanic and Atmospheric Research (MJM).

References

Arnault, S., 1987. Tropical Atlantic geostrophic currents and ship drifts. Journal of Geophysical Research 92, 5076–5088.

Ballabrera-Poy, J., Murtugudde, R., Busalacchi, A., 2002. On the potential impact of sera-surface salinity observations on ENSO predictions. Journal of Geophysical Research 107, 8007.

Bingham, F., Howden, S., Koblinsky, C., 2002. Sea surface salinity measurements in the historical database. Journal of Geophysical Research 107 (C12), 8019.

Boyer, T.P., Levitus, S., 2002. Harmonic analysis of climatological sea surface salinity. Journal of Geophysical Research, 8006.

Cronin, M., McPhaden, M., 1998. Upper ocean salinity balance in the western equatorial Pacific. Journal of Geophysical Research 103, 27,567–27,587.

Delcroix, T., 1998. Observed surface oceanic and atmospheric variability in the tropical Pacific at seasonal and ENSO time scales: a tentative overview. Journal of Geophysical Research 103, 18,611–18,633.

Delcroix, T., Hénin, C., 1991. Seasonal and interannual variations of sea-surface salinity in the tropical Pacific Ocean. Journal of Geophysical Research 96, 22135–22150.

Delcroix, T., McPhaden, M.J., 2002. Interannual sea surface salinity and temperature changes in the western Pacific warm pool during 1992–2000. Journal of Geophysical Research 107, 8002.

Delcroix, T., Picaut, J., 1998. Zonal displacement of the western equatorial Pacific fresh pool. Journal of Geophysical Research 103, 1087–1098.

Delcroix, T., Hénin, C., Porte, V., Arkin, P., 1996. Precipitation and sea-surface salinity in the tropical Pacific. Deep-Sea Research I 43, 1123–1141.

Deltel, C., Mercier, H., Weaver, A., 2004. Identifiability of climatological air-sea fluxes by a 4D-Var assimilation of seasonal hydrographic data. Quarterly Journal of the Royal Meteorological Society submitted for publication.

Denman, K., Freeland, H., 1985. Correlation scales, objective mapping, and a statistical test of geostrophy over the continental shelf. Journal of Marine Research 43, 517–539.

Dessier, A., Donguy, J.-R., 1994. The sea-surface salinity in the tropical Atlantic between 10°S and 30°N—seasonal and interannual variations (1977–1989). Deep-Sea Research I 41, 81–100.

Donguy, J.R., Hénin, C., 1976. Relations entre les précipitations et la salinité de surface dans l'océan Pacifique tropical sud-ouest basées sur un échantillonnage de surface de 1956 à 1973. Annales Hydrographiques 5, 53–59.

Donguy, J.-R., Meyers, G., 1996. Seasonal variations of sea-surface salinity and temperature in the tropical Indian Ocean. Deep-Sea Research I 43, 117–138.

Durand, F., Gourdeau, G., Delcroix, T., Verron, J., 2002. Assimilation of sea surface salinity in a tropical OGCM: a twin experiment approach. Journal of Geophysical Research 107 (C12), 8004.

Eldin, G., Rodier, M., Radenac, M.H., 1997. Physical and nutrient variability in the upper equatorial Pacific associated with westerly wind forcing and wave activity in October 1994. Deep-Sea Research I 44, 1783–1800.

Emery, W., Thomson, R., 1998. Data analysis methods in physical oceanography. Pergamon, Elsevier Science Ltd 634pp.

Freitag, H.P., McCarty, M.E., Nosse, C., Lukas, R., McPhaden, M.J., Cronin, M.F., 1999. COARE Seacat data: calibrations and quality control procedures. NOAA Technical Memorandum ERL PMEL-115, 89pp.

Gandin, L., 1963. Objective Analysis of Meteorological Fields. Hydrometeorological Service, Leningrad 286pp.

Gouriou, Y., Delcroix, T., 2002. Seasonal and ENSO variations of sea surface salinity and temperature in the South Pacific Convergence Zone during 1976–2000. Journal of Geophysical Research 107 (C12), 8011.

Grelet, J., Servain, J., Lorenzzetti, J., Vianna, M., 2003. Recueil de données météo-océaniques obtenues durant les campagnes PIRATA: années 1997–2003. Centre IRD de Brest, BP70, 29280 Plouzané, France, 88pp.

Han, W., McCreary, J., 2001. Modeling salinity distributions in the Indian Ocean. Journal of Geophysical Research 106, 859–877.

Hénin, C., Grelet, J., 1996. A merchant ship thermosalinograph network in the Pacific Ocean. Deep-Sea Research I 43, 1833–1856.

Hires, R., Montgomery, R., 1972. Navifacial temperature and salinity along the track from Samoa to Hawaii, 1957–1965. Journal of Marine Research 30, 177–200.

Johnson, G., Sloyan, B., Kessler, W., McTaggart, K., 2002a. Direct measurements of upper ocean currents and water properties across the tropical Pacific during the 1990s. Progress in Oceanography 52, 31–61.

Johnson, E., Lagerloef, G., Gunn, J., Bonjean, F., 2002b. Surface salinity advection in the tropical oceans compared with atmospheric forcing: a trial balance. Journal of Geophysical Research, 33.

Kashino, Y., Hase, H., Ando, K., Yoneyama, K., Takatsuki, Y., Kuroda, Y., Mizuno, K., 2001. Tropical Ocean Climate Study (TOCS) Data Report 2: 1995–2000. Ocean Japan Marine Science and Technology Center (JAMSTEC), Yokosuka, Japan 372pp.

Kerr, Y., Waldteufel, P., Wigneron, J.P., Martinuzzi, J.M., Font, J., Berger M, M., 2001. Soil moisture retrieval from space: the soil moisture and ocean salinity (SMOS) mission. IEEE Transactions on Geoscience and Remote Sensing 39 (8), 1729–1735.

Kessler, W., Taft, B., 1985. An assessment of the XBT sampling network in the central Pacific. University Corporation for Atmospheric Research, USTOGA 4, 62pp.

Kessler, W., Taft, B., 1987. Dynamic heights and zonal geostrophic transports in the central tropical Pacific during 1979–84. Journal of Physical Oceanography 17, 97–122.

Kessler, W., Spillane, M., McPhaden, M., Harrison, D., 1996. Scales of variability in the equatorial Pacific inferred from the TAO buoy array. Journal of Climate 9, 2999–3024.

Kobayashi, F., Takahashi, K., 2002. Distribution of diatoms along the equatorial transect in the western and Central

Pacific during the 1999 La Niña conditions. Deep-Sea Research I 49, 2801–2821.

Koblinski, C., Hildebrand, P., LeVine, D., Pellerano, F., Chao, Y., Wilson, W., Yueh, S., Lagerloef, G., 2003. Sea surface salinity from space: science goals and measurements approach. Radio Science 12, 38–44.

Kuragano, T., Kamachi, M., 2000. Global statistical space–-time scales of oceanic variability estimated from the Topex/Poseidon altimeter data. Journal of Geophysical Research 105, 955–974.

Kuroda, Y., Amitani, Y., 2001. TRITON : new ocean and atmosphere observing buoy network for monitoring ENSO. Umi no Kenkyu 10, 157–172 (in Japanese with English abstract).

Kuroda, Y., McPhaden, M., 1993. Variability in the western equatorial Pacific Ocean during Japanese Pacific climate study cruises in 1989 and 1990, 1993. Journal of Geophysical Research 98, 4747–4759.

Lagerloef, G., Delcroix, T., 2001. Sea surface salinity: a regional case study for the tropical Pacific. In: Observing the Ocean in the 21st Century. Australian Bureau of Meteorology, Melbourne, Australia, pp. 137–148.

Le Bec, N., Juillet-Leclerc, A., Correge, T., Blamart, D., Delcroix, T., 2000. A coral δ^{18}O record of ENSO driven sea surface salinity variability in Fiji (South-Western Tropical Pacific). Geophysical Research Letters 27, 3897–3900.

Levitus, S., 1982. Climatological Atlas of the World Ocean, NOAA Prof. Pap., 13. US Government Printing Office, Washington, DC 73pp.

Levitus, S., 1986. Annual cycle of salinity and salt storage in the world ocean. Journal of Physical Oceanography 16, 322–343.

Loukos, H., Vivier, F., Murphy, P., Harrison, D., Le Quéré, C., 2000. Interannual variability of equatorial Pacific CO_2 fluxes estimated from temperature and salinity data. Geophysical Research Letters 27, 1735–1738.

Maes, C., 1998. Estimating the influence of salinity on sea level anomaly in the ocean. Geophysical Research Letters 25, 3551–3554.

Mangum, L., Hayes, S., Stratton, L., 1992. Sampling requirements for the surface wind fields over the tropical Pacific Ocean. Journal of the Atmospheric and Oceanic Technology 9, 668–679.

Masson, S., Delecluse, P., 2001. Influence of the Amazon river runoff on the tropical Atlantic. Physics and Chemistry of the Earth 26, 137–142.

McPhaden, M.J., 1995. The TAO array is completed. Bulletin of the American Meteorological Society 76, 739–741.

McPhaden, M.J., Busalacchi, A., Picaut, J., 1988. A model study of potential sampling error due to scatter around XBT transects in the tropical Pacific Ocean. Journal of Geophysical Research 93, 8119–8130.

McPhaden, M.J., Freitag, P., Shepherd, A., 1990. Moored salinity time series measurements at 0°, 140°W. Journal of the Atmospheric and Oceanic Technology 4, 568–575.

McPhaden, M.J., Busalacchi, A.J., Cheney, R., Donguy, J.-R., Gage, K.S., Halpern, D., Ji, M., Julian, P., Meyers, G., Mitchum, G.T., Niiler, P.P., Picaut, J., Reynolds, R.W., Smith, N., Takeuchi, K., 1998. The Tropical Ocean–Global Atmosphere observing system: a decade of progress. Journal of Geophysical Research 103, 14169–14240.

Meyers, G., Philips, H., Smith, N., Sprintall, J., 1991. Space and time scales for optimal interpolation of temperature—Tropical Pacific Ocean. Progress in Oceanography 28, 189–218.

Mignot, J., Frankignoul, C., 2003. On the interannual variability of surface salinity in the Atlantic. Climate Dynamics 20, 555–565.

Neumann, G., 1969. Seasonal salinity variations in the upper strata of the western tropical Atlantic ocean, I. Sea surface salinities. Deep-Sea Research 16, 165–177.

Oberhuber, J., 1988. The budget of heat, buoyancy, and turbulent kinetic energy at the surface of the global ocean. An atlas based on the COADS data set. Report #15, Max Planck Institut für Meteorologie, Hamburg.

Picaut, J., Ioualalen, M., Delcroix, T., Masia, F., Murtugudde, R., Vialard, J., 2001. The oceanic zone of convergence on the eastern edge of the Pacific Warm Pool: a synthesis of results and implications for ENSO and biogeochemical phenomena. Journal of Geophysical Research 106, 2363–2386.

Prunier-Mignot, M., Varillon, D., Foucher, L., Ihily, J.-M., Buisson, B., Masia, F., Hénin, C., Ioualalen, M., Delcroix, T., 1999. Users Guide for Thermosalinograph Installation and Maintenance Aboard a Ship. Notes Techniques. Sciences de la Mer, Océanogr. Phys., Centre ORSTOM de Nouméa, New Caledonia, vol. 13, 102pp.

Rao, R., Sivakumar, R., 2003. Seasonal variability of sea surface salinity and salt budget of the mixed layer of the north Indian Ocean. Journal of Geophysical Research, 108.

Reverdin, G., Cayan, D., Dooley, H.D., Ellett, D.J., Levitus, S., du Penhoat, Y., Dessier, A., 1994a. Surface salinity of the North Atlantic: can we reconstruct its fluctuations over the last one hundred years ? Progress in Oceanography 33, 303–346.

Reverdin, G., Frankignoul, C., Kestenare, E., McPhaden, M.J., 1994b. A climatology of the seasonal currents in the equatorial Pacific. Journal of Geophysical Research 99, 20,323–20,344.

Roemmich, D., 2000. The Argo Project: global ocean observations for understanding and prediction of climate variability. Oceanography 13, 45–50.

Saur, J., 1980. Surface salinity and temperature on the San Francisco–Honolulu route, June 1966–December 1970 and January 1972–December 1975. Journal of Physical Oceanography, 1669–1680.

Servain, J., Busalacchi, A., McPhaden, M., Moura, A., Reverdin, G., Vienna, M., Zebiak, S., 1998. A pilot research moored array in the tropical Atlantic (PIRATA). Bulletin of the American Meteorological Society 79, 2019–2031.

Sprintall, J., Roemmich, D., 1999. Characterizing the structure of the surface layer in the Pacific Ocean. Journal of Geophysical Research 104, 23297–23311.

Stephens, C., et al., 2002. World Ocean Database 2001. In: Levitus, S. (Ed.), Temporal Distribution of C/STD Casts. NOAA Nesdis 44, vol. 3. US Government Printing Office, Washington, DC, p. 47.

Ueki, I., Ando, K., Kuroda, Y., Kutsuwada, K., 2002. Salinity variation and its effect on dynamic height along 156°E in the Pacific warm pool. Geophysical Research Letters, 29.

Vialard, J., Delecluse, P., Menkes, C., 2002. A modelling study of salinity variability and its effects in the tropical Pacific during the 1993–1999 period. Journal of Geophysical Research.

Wang, X., Chao, Y., 2004. Simulated sea surface salinity variability in the tropical Pacific. Geophysical Research Letters, 31.

WCRP, 1990. Scientific plan for the TOGA Coupled Ocean-Atmosphere Response Experiment, World Climate Research Program Publications Series #3, addendum, January 1990.

WCRP, 1998. CLIVAR initial implementation plan, World Climate Research Program Publications 103. WMO/TD 869, ICPO 14, June 1998.

White, W., Berstein R, R., 1979. Design of an oceanographic network in the mid-latitude North Pacific. Journal of Physical Oceanography 9, 592–606.

White, W., Meyers, G., Hasanuma, K., 1982. Space/time statistics of short-term climatic variability in the western North Pacific. Journal of Geophysical Research 87, 1979–1989.